NUREG/CR-0325

RELEVANCE OF FATIGUE TESTS TO COLD LEG PIPING

M. E. Mayfield E. C. Rodabaugh
R. J. Eiber

Battelle Columbus Laboratories

Prepared for
U. S. Nuclear Regulatory Commission

Available from
National Technical Information Service
Springfield, Virginia 22161
Price: Printed Copy $6.50 ; Microfiche $3.00

The price of this document for requesters outside of the North American Continent can be obtained from the National Technical Information Service.

NUREG/CR-0325
R5

RELEVANCE OF FATIGUE TESTS TO COLD LEG PIPING

M. E. Mayfield E. C. Rodabaugh
R. J. Eiber

Manuscript Completed: July 1978
Date Published: September 1978

Battelle Columbus Laboratories
505 King Avenue
Columbus, OH 43201

Division of Reactor Safety Research
Office of Nuclear Regulatory Research
U. S. Nuclear Regulatory Commission
Under Contract No. NRC-04-76-293-03

TABLE OF CONTENTS

TABLE OF CONTENTS
(Continued)

LIST OF TABLES

LIST OF FIGURES

LIST OF FIGURES
(Continued)

NOMENCLATURE

$C_i, K_i,\ i = 1,2,3$	=	Code Stress Indices
D_o	=	Outside Diameter, in.
E	=	Modulus of Elasticity, psi
h	=	Film Coefficient, Btu/hr-ft^2 - F
I	=	Moment of Inertia, in.^{4}
K_e	=	Simplified Elastic Plastic Analysis Correction Factor
K	=	Thermal Conductivity of Plate Material, Btu/hr-ft - F
M	=	Applied Moment Range, in.-lb
M	=	Material Parameter
n, m	=	Material Parameters as Given in NB-3228.3(b) of the Code
N_c	=	Code Allowable Number of Load Cycles
N_t	=	Number of Test Cycles When a Crack Penetrated Wall
N_t/N_c	=	Safety Margin
P_o	=	Applied Pressure Range, psi
R_m	=	Run Pipe Mean Radius, in.
S_y	=	Material Yield Strength at Design Temperature, psi
S_n	=	Primary plus Secondary Stress Intensity Range, psi
S_p	=	Peak Stress Intensity Range, psi
S_{alt}	=	Alternating Stress Intensity Range, psi
S_m	=	Design Stress Intensity Value, psi
ΔT	=	Absolute Temperature Range, F
T	=	Applied Temperature, F
T_r	=	Run Pipe Thickness, in.
t	=	Nominal Wall Thickness, in.
Z	=	Section Modulus, in.^{3}
α	=	Coefficient of Thermal Expansion
α_d	=	Thermal Diffusivity of Plate Material, ft^2/hr
δ	=	Plate Thickness, ft
θ	=	Time, hr
ν	=	Poisson's Ratio

RELEVANCE OF FATIGUE TESTS TO COLD LEG PIPING

by

M. E. Mayfield, E. C. Rodabaugh
and R. J. Eiber

1.0 INTRODUCTION

The "cold leg" in a PWR, for the purpose of this report, is defined as that portion of the primary coolant loop that lays between the coolant pump and the reactor vessel. One of the conditions which may lead to failure in a cold leg consists of repeated cycles of stress. These repeated stress cycles may cause the growth of any small defect in the weld or base material and, if the stress cycles are high enough and frequent enough, the defect may grow until it penetrates the wall, resulting in a leak, or under some postulated conditions, a large break might occur.

Over the past 30 years, many fatigue tests have been run on piping products.* With a few exceptions as noted later in this report, the tests were run on products that were small-scale models of components used in cold legs. In most tests, the test specimens represent random selection of stock items and the welding into test assemblies was not controlled to the extent required for the cold leg in PWRs. Accordingly, the test specimens usually represent a lower quality product than would be expected in cold legs of PWRs. With a few exceptions, tests were run at room temperature with an external air environment, internal ordinary tap water or air environment. The tests were run over a relatively short period of time (days or weeks) as compared to the postulated 40 year life of a PWR. Accordingly, the tests do not encompass environmental effects.

---

* A piping product is defined as anything in a piping system. Some examples:
(1) A length of seamless straight pipe, remote from welds or other discontinuities
(2) A girth butt weld between pipe and elbow
(3) An elbow
(4) A branch connection
(5) An ANSI B16.9 tee.

With a few exceptions, the test specimens did not contain any deliberately introduced defects. Such defects as did exist can be considered as typical of defects in the base material and weldments of piping products.

At present, the fatigue tests of piping products form the most important basis and justification for the fatigue evaluation procedures used today in the evaluation of cold legs in PWRs, as well as other nuclear power plant and industrial piping. The evaluation method is contained in the Code*; a discussion of the background of that method is included later herein.

1.1 Objective

The objective of this report is to present an evaluation of available fatigue test data on piping products to:

(1) Determine the margin of safety of the present ASME code method of evaluation.

(2) Determine the leak-rupture trends of components tested with significant internal pressures.

(3) Determine the implications of the tests with respect to the cold leg piping systems in PWR's.

1.2 Background of the ASME Code Fatigue Evaluation Method

Piping in nuclear power plants is designed in accordance with the Code. Piping which constitutes portions of the primary coolant pressure boundary are designed by Class 1 rules of the Code; specifically under NB-3600 of the Code. Because of the complexity of piping products, it has been found useful to establish "stress indices" and "flexibility factors" to describe, in a simple manner, the characteristics of such complex products; e.g., elbows or branch connections. These stress indices are contained in Table NB-3682.2-1 of the Code.

---

* Code, in this report, refers to the ASME Boiler and Pressure Vessel Code, Section III, Div. 1, "Nuclear Power Plant Components", Subsection NB, Reference (1)** herein.

** Numbers in parentheses ( ) denote references as listed in the Reference Section of this report.

A piping system analysis starts with an analysis of the system modeled as a one-dimensional assembly of straight and curved beams with appropriate restraints to represent anchors, guides, hangers, snubbers, etc. The behavior of complex piping products such as elbows is represented by flexibility factors incorporated into the system analysis model. Flexibility factors are given in NB-3687 of the Code. The piping system model is then "loaded" by the weight of piping, contents and insulation, by displacements representing the relative motion between restraints and by dynamic loadings induced by such effects as relief valve and earthquake induced motions. The piping system analysis is accomplished using computer programs that have been developed for that purpose. General purpose finite element computer programs can be used for a piping system analysis but usually it is more economical to use a special purpose program. The analysis is ordinarily an elastic analysis even though the loadings may induce a limited amount of plastic response in portions of the piping.

From the piping system analysis, one obtains loads at each restraint (e.g., the load on a pressure vessel nozzle or pump nozzle) and, of particular significance in this report, the moments* acting on the piping products. The loads on the piping system will have some (postulated in the design stage) time-dependent history, hence the moments will also have a time-dependent history and from this we can obtain the number of cycles of moments and magnitude of these moments. The cycles of moments are translated into cycles of stress by use of the Code stress indices, specifically those indices identified with a subscript "2" are for moment loading.

There are two other loadings which can produce significant cycles of stress in the piping; (1) internal pressure, and (2) thermal gradiants.

The history of pressure is normally postulated in the design stage, and by using the Code stress indices for pressure loading, identified by a subscript "1", the pressure history can be translated into cycles of stress due to cycles of pressure.

Evaluation of stresses due to thermal gradients follows from a "Heat Transfer" analysis in which the postulated cycles of fluid temperatures are

---

* A piping system analysis also gives axial forces acting on the piping and piping products but the effect of these on stresses in the piping and piping products are usually negligible.

translated into cycles of metal temperatures in the pressure boundary of the piping products. This analysis involves fluid temperature change rates, fluid velocities, film coefficients, etc. The cycles of metal temperatures are then characterized as certain types of gradients according to Code specified procedures as indicated in NB-3653 of the Code. These gradients, when multiplied by the thermal gradient stress indices (identified by a subscript "3") give the cycles of stresses due to thermal gradients.

The Code gives criteria to determine the acceptibility of the combinations of cyclic stresses due to cycles of moments, pressure, and thermal gradients. In the evaluation of the fatigue characteristics of piping components several calculated quantities are of interest. These variables are calculated based on the moment, pressure, and thermal stresses determined in the stress analysis as noted earlier. The equations used in calculating these variables are listed below.

(1) Primary Plus Secondary Stress Intensity Range

$$S_n = \frac{C_1 P_o D_o}{2t} + \frac{C_2 D_o M_i}{2I} + \frac{1}{2(1-\nu)} E\alpha \left| \Delta T_1 \right| + C_3 E_{ab} \left| \alpha_a T_a - \alpha_b T_b \right| , \quad (1)$$

(2) Peak Stress Intensity Range

$$S_p = K_1 C_1 \frac{P_o D_o}{2t} + K_2 C_2 \frac{D_o M_i}{2I} + \frac{1}{2(1-\nu)} K_3 E\alpha \left| \Delta T_1 \right| + K_3 C_3 E_{ab} \left| \alpha_a T_a - \alpha_b T_b \right| + \frac{1}{1-\nu} E\alpha \left| \Delta T_2 \right| . \quad (2)$$

(3) Alternating Stress Intensity

$$S_{alt} = K_e \frac{S_P}{2} \quad , \tag{3}$$

where,

$$K_e = 1.0 \text{ for } S_n \leq 3S_m$$

$$= 1.0 + \frac{(1 - n)}{n(m - 1)} \left(\frac{S_n}{3S_m} - 1 \right) \quad , \text{ for } 3S_m < S_n < 3m\, S_m$$

$$= \frac{1}{n} \quad \text{for } S_n \geq 3m\, S_m \quad , \tag{4}$$

with m and n being material parameters as given in NB-3228.3(b) of the Code and S_m the design stress intensity value for the material as given in Appendix I, Table 1-1.1 of the Code.

The values of the stress indices (K_i and C_i) are determined from Table NB-3682.2-1 of the Code.

The values of S_{alt} determined in this fashion represent an extrapolated elastic stress that should provide conservative estimates of the fatigue life of the component.

This Code evaluation procedure is an elastic type analysis. Combinations of loads that exceed the proportional limit of the component are treated as ficticious elastic loads (see Figure 1). Care must be taken in the evaluation of experimental results. Values of extrapolated elastic loads must be used to obtain evaluations compatible with elastic analysis.

The use of an elastic analysis and extrapolated elastic loads has been justified in the "Criteria of the ASME Boiler and Pressure Vessel Code for Design By Analysis In Sections III and VIII, Division 2"[(2)] which states:

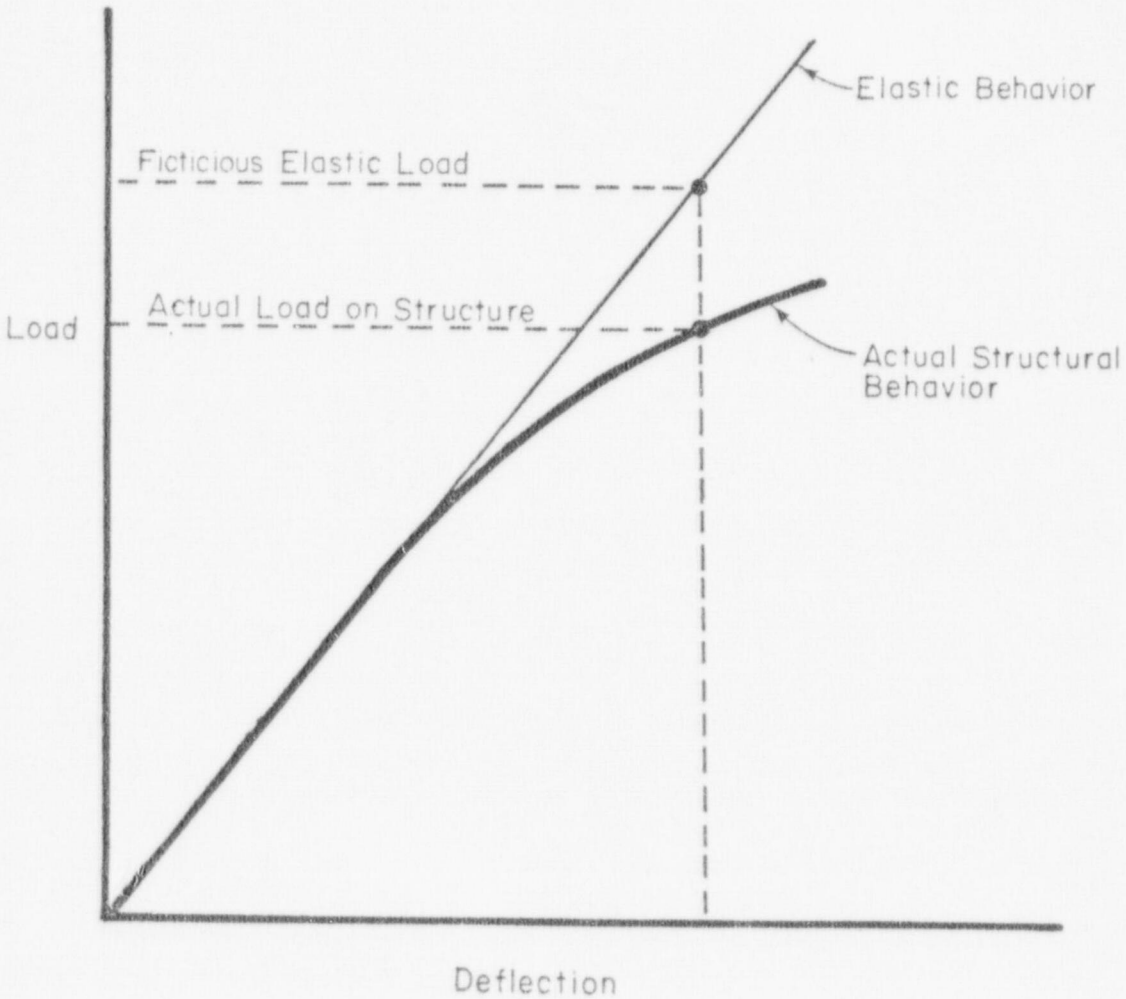

FIGURE 1. IDEALIZED LOAD-DEFLECTION CURVE

"Allowable stresses higher than yield appear in the values for primary-plus-secondary stress and in the fatigue curves. In the case of the former, the justification for allowing calculated stresses higher than yield is that the limits are such as to assure shake-down to elastic action after repeated loading has established a favorable pattern of residual stresses. Therefore the assumption of elastic behavior is justified because it really exists in all load cycles-subsequent to shake-down.

In the case of fatigue analysis, plastic action can actually persist throughout the life of the vessel, and the justification for the specified procedure is somewhat different. Repetitive plastic action occurs only as the result of peak stresses in relatively localized regions and these regions are intimately connected to larger regions of the vessel which behave elastically. A typical example is the peak stress at the root of a notch, in a fillet, or at the edge of a small hole. The material in these small regions is strain-cycled rather than stress-cycled and the elastic calculations give numbers which have the dimensions of stress but are really proportional to the strain. The factor of proportionality for uniaxial stress is, of course, the modulus of elasticity. The fatigue design curves have been specially designed to give numbers comparable to these fictitious calculated stresses. The curves are based on strain-cycling data and the strain values have been multiplied by the modulus of elasticity. Therefore stress intensities calculated from the familiar formulas of strength-of materials texts are directly comparable to the allowable stress values in the fatigue curves."

Once an appropriate value of S_{alt} is determined, the evaluation of the code allowable number of load cycles (N_c) can be made through the use of the S-N curves shown in Figures 2 and 3 of this report (Figures 1.9.1 and 1.9.2 of the Code).[3]

The procedure, outlined above, for determining the Code design life was employed in evaluating a "margin of safety" (N_t/N_c), where N_t is the number of load cycles applied prior to the detection of a leak, for the

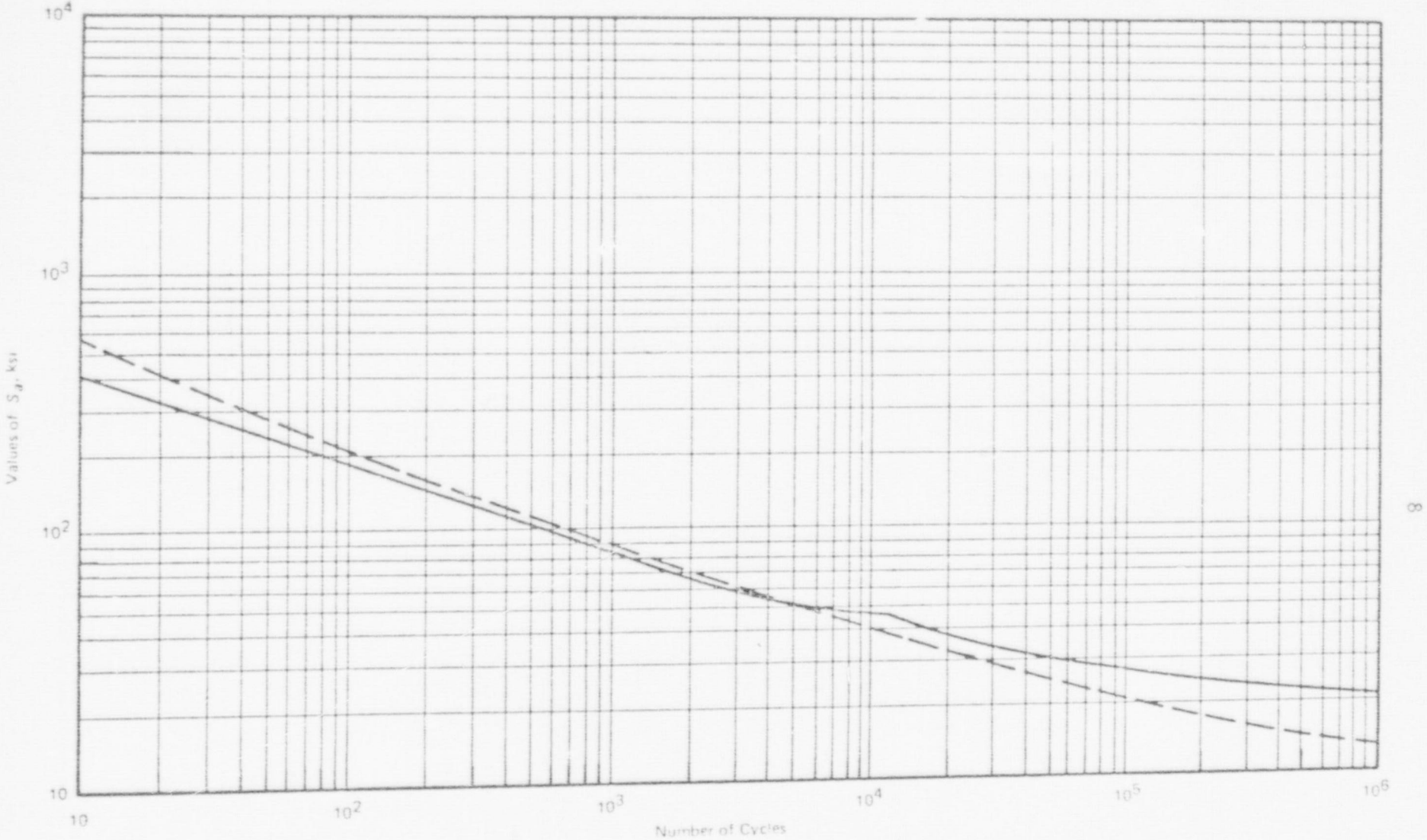

NOTE: $E = 30 \times 10^6$ ksi

— — UTS ≤ 80.0 ksi

——— UTS 115.0-130.0 ksi

Interpolate for UTS 80.0–115.0 ksi

FIGURE 2. DESIGN FATIGUE CURVES FOR CARBON, LOW ALLOY, AND HIGH TENSILE STEELS
(For Metal Temperatures Not Exceeding 700 F)

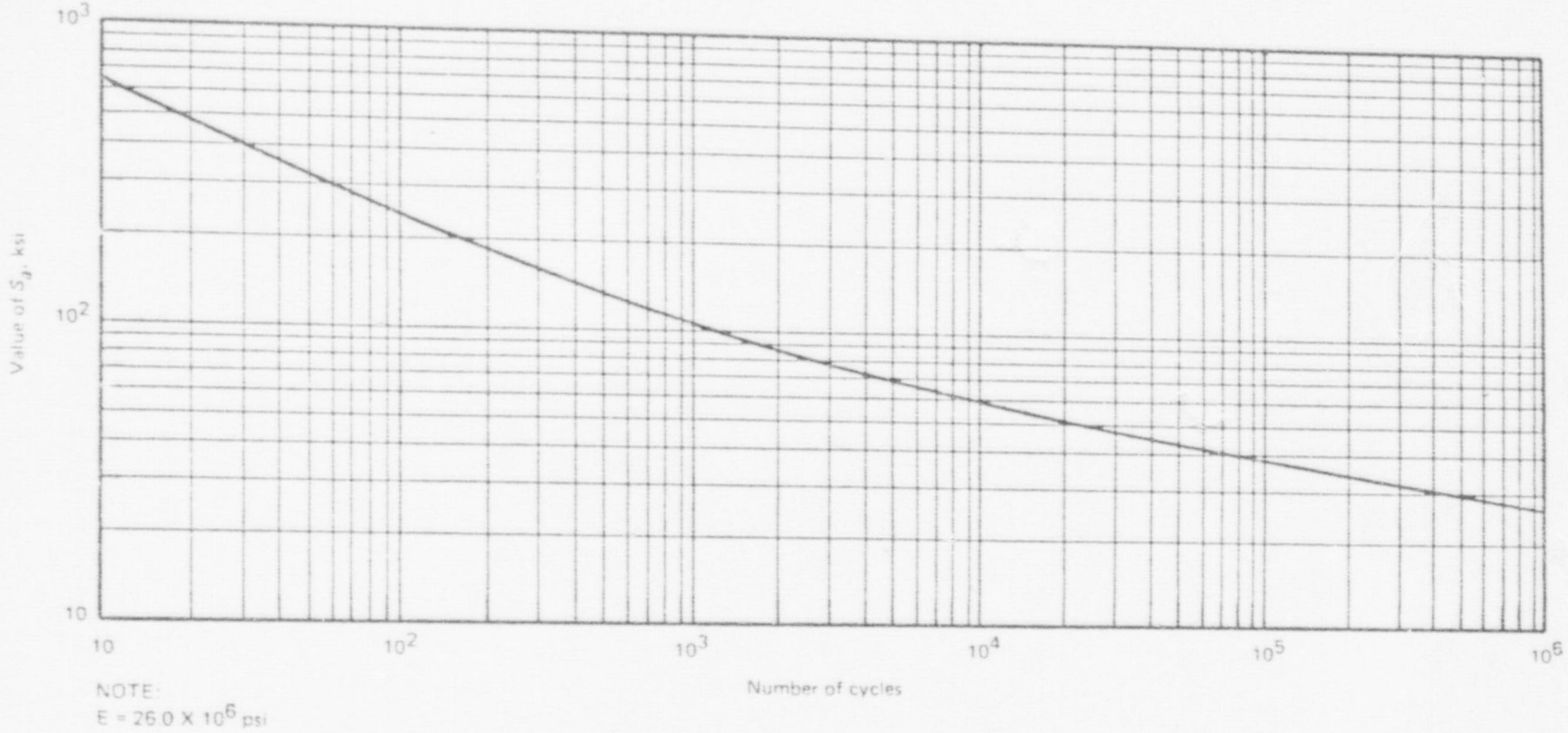

FIGURE 3. DESIGN FATIGUE CURVE FOR AUSTENITIC STEELS, NICKEL-CHROMIUM-IRON ALLOY, NICKEL-IRON-CHROMIUM ALLOY, AND NICKEL-COPPER ALLOY

fatigue test results given in Section 2 of this report. Following the example given in Reference (10) a conservative value for N_t/N_c is taken as 20 which is the Code safety factor incorporated into Figures 2 and 3.

Reference (10) gives an analysis of the test fatigue lives of piping components as compared to the Code methods in use at the time they were prepared. This report expands that analysis to correspond to the Code (1977) method and to include recent test data (when possible) and attempts to make some assessment of the implications such small-scale tests may have on the PWR cold leg piping.

2.0 EVALUATION OF FATIGUE LIVES IN TERMS OF N_t/N_c

2.1 Girth Butt Welds

Evaluation of tests on girth butt welds are summarized in Table 1. With the following exceptions, all welds are assumed to have been made by a 'good' welder and are thereby comparable.

Four tests from Reference (7) on girth butt welds are shown in Table 1. These are classified as:

Identification	Pipe Material	Weld	Test Temperature
HW-1	A-106-B, carbon steel	Good	550 F
HWD-1	A-106-B, carbon steel	Defective	"
HW-3A	304 stainless steel	Good	"
HWD-3	304 stainless steel	Defective	"

The "defective" welds had an intentional defect; a lack of penetration produced by not completing a 1-inch section of root pass. Presumably the defect was aligned with the maximum bending stress during the test.

These two tests represent a significant piece of information in that the Code analysis did not become completely nonconservative when applied to a flawed component. These tests are incorporated into Table 1. The same analysis technique was used for all tests considered.

As will be discussed, the results of these tests, in terms of N_t/N_c and the applied stress level, are somewhat erratic. However, when comparing results for carbon steel to those for stainless steel certain trends may be noted.

It will be noted that for the 550 F tests the values of N_t/N_c for the carbon steels range from 14.3 to 128.4 for the unflawed test specimens. The range of N_t/N_c for the stainless steel tests is from 6.3 to 76.6 again for unflawed test specimens. For the flawed specimen tests, the carbon steel N_t/N_c = 6.8 while N_t/N_c for the stainless steel test is 1.9. In both the flawed and unflawed condition, the analysis for carbon steel components (at

TABLE 1. EVALUATION OF FATIGUE TESTS ON GIRTH BUTT WELDS WITH CYCLIC MOMENT LOADINGS

Ref. No.	Type of Component	M/Z, ksi	S_n, ksi	$\frac{S_n}{3S_m}$	S_p, ksi	K_e	$\frac{K_e S_p}{2}$, ksi	N_c	Test N_t	$\frac{N_t}{N_c}$
(6) Fig. 5 (1)	Girth butt weld 4" std. wt.	90.0	90.0	1.50	162.0	2.00	162.0	190	2,500 to 3,500	13.0 to 18.0**
(7) HW-1	Girth butt weld 6" std. wt., A-106-B	58.2	58.2	1.08	105.0	1.16	60.8	2500	35,740	14.3
(7) HWD-1	Girth butt weld* 6" std. wt., A-106-B	59.2	59.2	1.10	107.0	1.20	64.2	2000	13,600	6.8*
(7) HW-3A	Girth butt weld 6" std. wt., Type 304	61.1	61.1	1.272	110.0	1.905	105.0	1100	6,950	6.3
(7) HWD-3	Girth butt weld* 6" std. wt., Type 304	59.9	59.9	1.247	107.8	1.823	98.5	1400	2,600	1.9*
(9) CS-160-1 (2)	Girth butt weld 6" sch. 160, A-106-B	101.6	101.6	1.694	182.9	3.313	303.1	55	7,456	135.6
(9) CC-160-1 (2)	Girth butt weld 6" sch. 160, Type 304	95.8	95.8	1.596	172.5	2.19	189.0	130	7,724	59.4
(9) CC-80-1 (2)	Girth butt weld 6" sch. 80, A-106-B	119.4	119.4	1.99	214.9	2.98	320.3	35	>1,713	>48.9
(9) HW-15	Girth butt weld 6" sch. 80, A-106-B	117.6	117.6	2.26	211.8	3.52	372.7	25	3,209	128.36

TABLE 1. (Continued)

Ref. No.	Type of Component	M/Z, ksi	S_n, ksi	$\frac{S_n}{3S_m}$	S_p, ksi	K_e	$\frac{K_e S_p}{2}$, ksi	N_c	Test N_t	$\frac{N_t}{N_c}$
(9) HW-14	Girth butt weld 6" sch. 80, A-106-B	87.3	87.3	1.68	157.2	2.36	185.5	140	7,278	51.98
(9) HW-12	Girth butt weld 6" sch. 80, Type 304	93.8	93.9	1.9	169.	3.33	281.7	70	2,894	41.3
(9) HW-11	Girth butt weld 6" sch. 80, Type 304	64.2	64.2	1.3	115.5	2.0	115.6	680	14,858	21.85
(9) HW-10	Girth butt weld 6" sch. 80, Type 304	79.0	79.0	1.6	142.4	3.0	213.5	120	9,200	76.6

* Specimen had an intentional defect, see text.

** Range of N_t/N_c for three test specimens.

(1) These components were tested at room temperature with no internal pressure.

(2) These components were tested at room temperature with a constant internal pressure of 1050 psig for CC-80-1 and 2200 psig for CC-160-1 and CS-160-1. All other specimens were tested at 550 F with no internal pressure.

550 F) is more conservative than the analysis for the stainless steel components.

Although the data presented for the room temperature tests is insufficient to allow any valid comparisons, it may be that the trend is reversed, i.e., that the analysis for stainless steel is more conservative at room temperature than is the analysis for carbon steel.

2.2 Short-Radius and Long-Radius Elbows

Table 2 lists the results of fatigue tests on short-radius and long-radius elbows. The pertinent test parameters for each component are shown in the table.

The majority of the tests used cyclic moment loadings. A few tests also employed a constant internal pressure (the pressure is noted in Table 2). Two tests (CSLS-5 and CSLS-7) used a combined cyclic moment load and a cyclic pressure load.

The last entry in Table 2 is the specimen ORNL-ME-2[4]. This test used cyclic pressure loading with no cyclic moment. The specimen was intentionally deformed so that it was 5.7 percent out-of-round. The Code allowable number of cycles was determined considering the out-of-round conditions.[5] Unfortunately, the limits of the test apparatus would have been exceeded if the test went past 100,000 cycles. Therefore, the test was terminated at 50,000 cycles. Strain gage data indicated that the code stress analysis was conservative. The authors note; "A careful post-test examination of the elbow did not reveal any cracks or any indication of fatigue crack initiation. Thus, although the test was continued only long enough to prove a safety factor of 10 rather than 20, we feel that the test results confirm the adequacy of the present Code rule".[4] Because this elbow was pressure cycled only, it will not be considered in the following analysis.

In examining Table 2 the following trends are noted.

(1) For an internal pressure equal to zero and a test temperature equal to the ambient room temperature, the values of N_t/N_c for stainless steel elbows ranged from 47 to 170 while the N_t/N_c values for carbon steel ranged from 118 to 2500. These ranges imply that the analysis is more conservative for carbon steel than for stainless steel.

TABLE 2. EVALUATION OF FATIGUE TESTS ON SHORT-RADIUS AND LONG-RADIUS ELBOWS

Ref. No.	Type of Component	ΔP_o, psi	M/Z, ksi	S_n, ksi	$\frac{S_n}{3S_m}$	S_p, ksi	K_e	$\frac{K_e S_p}{2}$, ksi	N_c	Test N_t	$\frac{N_t}{N_c}$
(6) Fig. 6	Short-radius elbow 4" std. wt. C.S.	0	100.0	554.0	9.24	554.0	5.00	1,380.0	<< 10	300 to 350	>> 30
(6) Fig. 6	Short-radius elbow 4" std. wt. C.S.	0	56.0	310.0	5.17	310.0	5.00	775.0	< 10	1,200 to 3,000	> 120
(6) Fig. 6	Short-radius elbow 0.072" wall C.S.	0	20.0	250.0	4.17	250.0	5.00	625.0	≈ 10	2,800	≈ 280
(6) Fig. 7	Short-radius elbow 4" std. wt. C.S.	0	56.0	310.0	5.17	310.0	5.00	775.0	< 10	2,800	> 280
(6) Fig. 7	Short-radius elbow 0.072" wall C.S.	0	30.0	375.0	6.25	375.0	5.00	935.0	< 10	5,000	> 500
(6) Fig. 7	Short-radius elbow 0.072" wall C.S.	0	20.0	250.0	4.17	250.0	5.00	625.0	≈ 10	15,000	≈ 1500
(7) CCLS-1	Short-radius elbow 6" std. wt. C.S. P=1050	0	43.6	280.0	4.67	280.0	5.00	700.0	< 10	1,176	> 118
(7) CCLS-2	Short-radius elbow 6" std. wt. C.S. P=1050	0	42.6	274.0	4.57	274.0	5.00	685.0	< 10	7,899	> 790
(7) CSLS-2	Short-radius elbow 6" std. wt. S.S. P=1050	0	42.2	272.0	4.54	272.0	3.33	454.0	22	6,838	310
(7) CSLS-1	Short-radius elbow 6" std. wt. S.S. P=1050	0	44.2	284.0	4.75	284.0	3.33	473.0	20	907	45
(7) HCLS-1 (1)	Short-radius elbow 6" std. wt. C.S.	0	43.5	280.0	5.20	280.0	5.00	700.0	< 10	760	> 76
(7) HCLS-2 (1)	Short-radius elbow 6" std. wt. C.S.	0	43.1	278.0	5.15	278.0	5.00	695.0	< 10	26,100	> 2600

TABLE 2. (Continued)

Ref. No.	Type of Component	ΔP_o, psi	M/Z, ksi	S_n, ksi	$\frac{S_n}{3S_m}$	S_p, ksi	K_e	$\frac{K_e S_p}{2}$, ksi	N_c	Test N_t	$\frac{N_t}{N_c}$
(7) HSLS-1 (1)	Short-radius elbow 6" std. wt. S.S.	0	28.0	180.0	3.75	180.0	3.33	700.0	56	2,200	39
(7) HSLS-2 (1)	Short-radius elbow 6" std. wt. S.S.	0	42.2	271.0	5.65	271.0	3.33	452.0	22	1,870	85
(6) Fig. 8	Long-radius elbow 4" std. wt. C.S.	0	50.0	212.0	3.54	212.0	5.00	530.0	12	2,500 to 20,000	210 to 1700
(6) Fig. 8	Long-radius elbow, 4" 0.16" wall C.S.	0	24.0	179.0	2.98	179.0	4.96	445.0	17	2,000	118
(6) Fig. 9	Long-radius elbow 4" std. wt. C.S.	0	86.0	365.0	6.08	365.0	5.00	910.0	<10	2,500	>2500
(6) Fig. 9	Long-radius elbow, 4" 0.101" wall C.S.	0	29.0	216.0	3.60	216.0	5.00	540.0	11	5,000	450
(7) CSLS-3	Long-radius elbow 6" std. wt. S.S.	0	44.2	217.0	3.62	217.0	3.33	362.0	35	4,469	128
(10) Fig. 7	Long-radius elbow, 4" std. wt. C.S. P=2,200	0	74.0	313.0	5.21	313.0	5.00	785.0	<10	1,300	>130
(10) Fig. 8	Long-radius elbow, 4" std. wt. C.S. P=2,200	0	80.0	338.0	5.64	338.0	5.00	845.0	<10	700	>70
(9) CSLS-5*	Long-radius elbow 6" std. wt. S.S.	1,375	49.9	266.1	5.34	266.1	3.33	443.5	25	3,990	159.6
(9) CSLS-7*	Long-radius elbow 6" std. wt. S.S.	2,800	44.7	262.2	5.33	262.2	3.33	436.9	24	2,531	105.5
(12) Curved Pipe #1***	Short-radius elbow, 8" 0.322" wall S.S.	0	234.4	1,594.3	26.57	1594.3	3.33	2,654.6	≈1	47	≈47

TABLE 2. (Continued)

Ref. No.	Type of Component	ΔP_o, psi	M/Z, ksi	S_n, ksi	$\frac{S_n}{3S_m}$	S_p, ksi	K_e	$\frac{K_e S_p}{2}$, ksi	N_c	Test N_t	$\frac{N_t}{N_c}$
(12) Curved Pipe #2***	Short-radius elbow, 8" 0.322" wall S.S.	0	127.5	866.9	14.45	866.9	3.33	1,444.8	↶2.5	230	92
(12) Curved Pipe #3***	Short-radius elbow, 8" 0.322" wall S.S.	0	75.3	512.7	8.546	512.7	3.33	854.6	↶7	615	87.8
(12) Curved Pipe #4***	Short-radius elbow, 8" 0.322" wall S.S.	0	30.98	208.0	1.73	208.0	3.33	346.7	42	7,110	169.3
(4) ORNL-ME-2**	Long-radius elbow, 10" 0.384" wall, C.S. out-of-round by 5.7%	0 2,200	0	38.8	.65	93.55	1	46.8	5200	>50,000**	>9.6

* Elbows subjected to cyclic pressure loading and moment loading.
** Test stopped at N = 50,000 cycles, see text.
*** The moment used is an extrapolated elastic moment.

(1) These components were tested at 550 F.
All others were room temperature tests.

C.S. = carbon steel
S.S. = stainless steel

(2) For internal pressures not equal to zero and an ambient test temperature, the N_t/N_c values for stainless steel ranged from 45 to 310 while the carbon steel values ranged from 118 to 790. These ranges imply that the analysis is again more conservative for carbon steel than for stainless steel. However, it may be noted that the total range of N_t/N_c values for the carbon steel was reduced while the range for the stainless steel tests was increased.

(3) There is insufficient data to make a valid assessment of the effect of elevated test temperature on N_t/N_c for the two classes of material.

2.3 Forged Welding Tees With Cyclic Moment Loadings

Table 3 lists the results of cyclic moment fatigue tests on forged welding tees. All of the tests listed in this table were conducted at room temperature.

The test parameters of interest are material type, stress level, and internal pressure. The material type and stress level (M/Z) are given in Table 3. The internal pressures are listed below.

Identification	Pressure (psig)
CSTS-1	1050
CSTS-2	1050
CSTS-3	1050
CCTS-1	1050
CCTS-2	1050
T-4, T-6, T-7, T-8, T-10, T-15	Design pressure calculated by $P = \frac{2 S_m (t_m - a)}{D_o - 0.8 (t_m - a)}$, with $t_m = 0.875$ times the nominal wall thickness and a=0.
T-16	300
All others	0

TABLE 3. EVALUATION OF FATIGUE TESTS ON FORGED WELDING TEES WITH MOMENT LOADING

Ref. No.	Type of Component[a]	M/Z,[b] ksi	S_n, ksi	$\frac{S_n}{3S_m}$	S_p, ksi	K_e	$\frac{K_e S_p}{2}$, ksi	N_c	Test N_t	$\frac{N_t}{N_c}$
(6) Fig. 10	Forged welding tee 4" std. wt.	100.0	290.0	4.85	290.0	5.00	725.0	< 10	900	> 90
(6) Fig. 10	Forged welding tee 4" std. wt.	86.0	250.0	4.17	250.0	5.00	625.0	≈ 10	1,500 to 5,000	150 to 500
(6) Fig. 11	Forged welding tee 4" std. wt.	104.0	300.0	5.00	300.0	5.00	750.0	< 10	1,500	> 150
(6) Fig. 11	Forged welding tee 4" std. wt.	86.0	250.0	4.17	250.0	5.00	625.0	< 10	700 to 4,000 to	> 70
(7) CSTS-1	Forged welding tee* 6" std. wt.	68.7	232.0	3.87	232.0	3.33	580.0	≈ 10	4,575	≈ 460
(7) CSTS-2	Forged welding tee* 6" std. wt.	67.8	229.0	3.84	229.0	3.33	574.0	≈ 10	3,310	≈ 330
(13) T-4	Forged welding tee 12" sch. 80	54.5	155.0	2.57	155.0	4.14	321.0	38	2,070	55
(13) T-7	Forged welding tee* 12" sch. 160	76.3	137.0	2.28	137.0	3.33	228.0	110	11,475	104
(13) T-8	Forged welding tee* 12" x 6" sch. 40	74.6	307.0	5.12	307.0	3.33	511.0	16	8,249	510
(13) T-10	Forged welding tee 24" sch. 40	44.0	194.0	3.23	194.0	5.00	485.0	15	18,532	1,200
(13) T-15	Forged welding tee* 12" x 6" sch. 40	72.3	297.0	4.95	297.0	3.33	495.0	18	11,803	660

TABLE 3. (Continued)

Ref. No.	Type of Component[a]	M/Z,[b] ksi	S_n, ksi	$\frac{S_n}{3S_m}$	S_p, ksi	K_e	$\frac{K_e S_p}{2}$, ksi	N_c	Test N_t	$\frac{N_t}{N_c}$
(9) CSTS-3	Forged welding tee* 6" std. wt.	72.7	246.3	5.0	246.3	3.33	410.5	27	3,675	136.1
(9) CCTS-1	Forged welding tee 6" std. wt.	68.2	230.9	3.848	230.9	5.00	577.3	<10	21,079	>2,107.9
(9) CCTS-2	Forged welding tee 6" std. wt.	70.6	239.2	3.986	239.2	5.00	597.9	<10	9,367	>936.7
(15) T-16	Forged welding tee* 24" x 24" x 24"	66.0	580.3	11.58	580.3	3.33	966.2	5	2,344	470
(13) T-6	Forged welding tee 12" x 12" x 12"	62.7	178.9	2.982	178.9	4.96	444.2	18	1,309	72.7

(a) All tees were ASTM A106 Grade B carbon steel material, except those with an asterisk; these were Type 304 austenitic stainless steel material.

(b) Z is the section modulus of the branch pipe for those tees in which the branch is smaller than the run.

Note: All tests were conducted at room temperature.

For both the pressurized and unpressurized conditions, the Code analysis method is more conservative for the carbon steel specimens than for the stainless steel specimens. The range of N_t/N_c values for the carbon steel tees was from 55 to 2100. The values for the stainless steel tees ranged from 104 to 660. There are no well defined relationships between sizes or stress level and the N_t/N_c factor.

2.4 Fabricated and Drawn Outlet Tees With Cyclic Moment Loading

Table 4 lists the results of cyclic moment fatigue tests on fabricated and drawn outlet tees.

In each case, the internal pressure was equal to zero and the test temperature was room temperature.

For these components, the Code analysis technique was more conservative for carbon steels than for stainless steels.

The test results fall into three groups in terms of material type and loading type, i.e., (R, L, D), (In-plane 1, 2, 3, 4), and (Out-of-plane 1, 2, 3, 4).

Group I (consisting of components designated R, L, and D) were all carbon steel tees. There appears to be a relationship between the magnitude of the M/Z term and the N_t/N_c factor. Specifically, for M/Z = 13.44 ksi the 'safety factor' is N_t/N_c increases to 1700, implying that the Code analysis becomes more conservative as the M/Z term increases. Considering Group II (In-plane 1, 2, 3, and 4) and Group III (Out-of-plane 1, 2, 3, and 4), it may be noted that the opposite trend is true for stainless steels. In Group II the M/Z term varies from 132.9 ksi to 66.9 ksi with the corresponding N_t/N_c values changing from 48 to 321.7. Similarly in Group III, M/Z varies from 77.8 ksi to 47.3 ksi while N_t/N_c varies from 24.5 to 254.8.

A second trend is evident in the comparisons of Groups II and III for a given M/Z level. The M/Z for test designation In-plane 3 is 78.8 ksi while that for test designation Out-of-plane 1 is 77.8 ksi (nearly the same value). The N_t/N_c values are 79.7 and 24.5, respectively. A similar trend is noted in comparing In-plane 4 and Out-of-plane 2. These values indicate that the Code analysis is sensitive to load type, i.e., the analysis is more conservative for in-plane loadings than for out-of-plane loadings.

TABLE 4. EVALUATION OF FATIGUE TESTS ON FABRICATED AND DRAWN OUTLET TEES WITH CYCLIC MOMENT LOADING

Ref. No.	Type of Component	M/Z, ksi	S_n, ksi	$\frac{S_n}{3S_m}$	S_p, ksi	K_e	$\frac{K_e S_p}{2}$, ksi	N_c	Test N_t	$\frac{N_t}{N_c}$
(16) R	Fabricated tee, 20 x 12	43.44	94.0	1.57	94.0	2.14	100.0	650	~80,000	~ 123
(16) L	Drawn outlet tee, 20 x 6	46.60	142.0	2.37	142.0	3.74	266.0	55	95,000	1,700
(16) D	Drawn outlet tee, 20 x 12	26.88	188.0	3.14	188.0	5.00	470.0	15	20,000	1,300
(12) In-plane 1	Fabricated*[(a)] tee	132.9	485.3	8.088	485.3	3.33	808.8	< 10	480	>48.0
(12) In-plane 2	Fabricated*[(a)] tee	81.7	298.4	4.97	298.4	3.33	497.3	18	840	46.6
(12) In-plane 3	Fabricated*[(a)] tee	78.8	287.6	4.79	287.6	3.33	479.3	22	1,755	79.7
(12) In-plane 4	Fabricated*[(a)] tee	66.9	244.4	4.074	244.4	3.33	407.4	28	9,007	321.7
(12) Out-of-plane 1	Fabricated*[(a)] tee	77.8	283.9	4.733	283.9	3.33	473.3	23	563	24.5
(12) Out-of-plane 2	Fabricated*[(a)] tee	67.9	248.0	4.134	248.0	3.33	413.4	26	1,945	74.8
(12) Out-of-plane 3	Fabricated*[(a)] tee	57.1	208.5	3.475	208.5	3.33	347.5	44	5,600	127.3
(12) Out-of-plane 4	Fabricated*[(a)] tee	47.3	172.6	2.875	172.6	3.33	287.5	73	18,600	254.8

* Indicates Type 304 stainless steel.

(a) Components are assumed to be tee sections, although the original report is not clear on this point.

Note: All tests were conducted at room temperature.

It should be noted that N_t/N_c was greater than 20 for every test listed in Table 4. The 'worst' case was for Out-of-plane 1, which had the highest out-of-plane loading and was made of stainless steel.

2.5 Forged Welding Tees, Fabricated Tees, and Unreinforced Branch Connections With Cyclic Internal Pressure Loading

Table 5 lists the results of internal pressure loading fatigue tests on forged tees (B16.9 type tees) fabricated tees, and unreinforced branch connections.

The tests may be divided into three groups. Group I (T-11, 12, and 13) were forged tees meeting the B16.9 specification.

Group II (Internal Pressure 1, 2, 3, and 4) were fabricated tees. It has been assumed that these tee sections (actually they are a type of branch connection) meet the Code requirements (NB-3643). The original reference indicates that the wall-thickness in the branch region was increased but does not provide sufficient information to make an accurate determination. If this assumption is incorrect and the specimens in fact did not meet the requirements of NB-3643 then the N_c term would be reduced implying a larger N_t/N_c. Thus the assumptions made herein represent a 'worst case' analysis.

Group III consists of two unreinforced branch connections (thin and thick branch). Because these branch connections were not reinforced, a reduced wall-thickness (T_r) was computed and used in evaluating the stress indices. T_r was computed from Equation 5.

$$T_r = T\left[\frac{1 + (t/T)\sqrt{x}}{2 + (d/D)\sqrt{x}}\right], \qquad (5)$$

where,

$$x = (d/t)/\left[2(d/t - 1)^2\right],$$

with

T = run pipe wall-thickness

t = branch pipe wall-thickness

D = run pipe diameter

d = branch pipe diameter.

TABLE 5. EVALUATION OF FATIGUE TESTS ON TEES AND BRANCH CONNECTIONS WITH CYCLIC INTERNAL PRESSURE LOADING

Ref. No.	Type of Component	$\frac{P D_o}{2t}$, ksi	S_n, ksi	$\frac{S_n}{3S_m}$	S_p, ksi	K_e	$\frac{K_e S_p}{2}$, ksi	N_c	Test N_t	$\frac{N_t}{N_c}$
(15) T-11	Forged tee[a] 24 x 24 x 24	35.2	53.0	0.7583	212.0	1.0	106.0	550	2,875	5.2
(15) T-12	Forged tee[b] 24 x 24 x 10	31.5	47.2	0.6747	188.6	1.0	94.3	750	76,620	102.2
(15) T-13	Forged tee[a] 24 x 24 x 10	33.0	49.5	0.7074	197.8	1.0	98.9	550	15,084	27.4
(12) Internal Pressure 1	Fabricated tee[c] 8 x 8 x 8	68.0	136.0	2.266	231.2	3.33	385.4	34	5,806	170.8
(12) Internal Pressure 2	Fabricated tee[c] 8 x 8 x 8	58.3	116.6	1.943	198.2	3.33	330.3	45	16,642	369.8
(12) Internal Pressure 3	Fabricated tee[c] 8 x 8 x 8	54.9	109.9	1.833	186.9	3.33	311.6	53	18,206	343.5
(12) Internal Pressure 4	Fabricated tee[c] 8 x 8 x 8	48.58	97.2	1.619	165.2	3.063	252.9	80	20,000	250.0
(17) Thin Branch	Un-reinforced Branch* (d)	48.42	96.85	1.61	164.7	2.22	182.8	120	3,543	29.5
(17) Thick Branch	Un-reinforced Branch* (d)	41.95	83.9	1.398	142.7	1.797	128.2	330	20,678**	62.6

(a) Material used: A-105 Grade 2.
(b) Material used: A-515 Grade 70.
(c) Material used: AISI 304.
(d) Low carbon steel (BS3601/27HFS). Assumed similar to A-106-B.

* Calculations based on reduced thickness T_r, see text for explanation.
** Component was intentionally flawed, see text.

Note: All tests were conducted at room temperature.

The configuration used in testing the Thick Branch and Thin Branch connections involved having both branches in a single run pipe. When the Thin Branch connection failed, it was removed and an intentional defect was introduced in the crotch region of the Thick Branch. The test was then resumed and continued until the connection failed.

All the tests listed in Table 5 were conducted at room temperature. The only loading applied was a cyclic internal pressure.

The general trend indicates that the analysis was more conservative for the stainless steel specimens than for the carbon steel specimens. This trend is opposite that observed in the previous sections. Because these results all come from one group of tests, it would be dangerous to place too much emphasis on this observed trend.

The results of the T-11 test are of much greater interest. The N_t/N_c value calculated was 5.2. This is in agreement with the analysis of Hayes and Moore.[15] Because these tees were 'off the shelf' items, it must be concluded that the fatigue analysis for pressure cycle loading is questionable. A need for review of the code design procedure for cyclic pressure loading is indicated.

2.6 Girth Fillet Welds

This report includes no tests in addition to those reported in Phase Report Number 115-10[10] for girth fillet welds. The table (Table 6) and the analysis contained in that report are included here for the sake of completeness.

Markl and George[18] give results of tests on fillet welds made between 4-inch pipe and 300-pound ASA B16.5 flanges. Such fillet welds are assigned a C_2-index of 2.1, K_2-index of 2.0 by the Code. These tests, like those of References (6) and (11), were displacement-controlled and fatigue failure was defined as the occurrence of leakage (crack through-the-wall).

Evaluation of these tests is shown in Table 6. As indicated by the last column of Table 6, the ratios of N_t/N_c, with one exception, are greater than 20. The one exception consisted of a "minimum" weld, described by the authors of Reference (18) as "the welds. . . were meant to represent the least

TABLE 6. EVALUATION OF FATIGUE TESTS ON GIRTH FILLET WELDS WITH MOMENT LOADING

Ref. No.	Type of Component	$\frac{M}{Z}$	S_n	$\frac{S_n}{3S_m}$	S_p	K_e	$\frac{K_e S_p}{2}$	N_c	Test N_t	$\frac{N_t}{N_c}$
(18) Fig. 7	Fillet welded girth joint	100,000	150,000	2.50	300,000	4.0	600,000	~10	87 to 1,200	8.7 to 120
(18) Fig. 7	Fillet welded girth joint	90,000	135,000	2.25	270,000	3.50	472,000	16	1,200 to 3,000	190
(18) Fig. 8	Fillet welded girth joint	116,000	174,000	2.90	348,00	4.80	835,000	<10	1,200	> 120
(18) Fig. 8	Fillet welded girth joint	90,000	135,000	2.25	270,000	3.50	472,000	16	339 to 2,800	21 to 170
(18) Fig. 9	Fillet welded girth joint	116,000	174,000	2.90	348,000	4.80	835,000	<10	750 to 830	> 75

weld size and quality compatible with code* requirements, were small (the weld size on hub fillets was of the order of 5/16-inch to 3/8-inch) and of a beadlike, unfinished appearance". One of two such specimens (shown in the first line of Table 6) tested at a nominal stress range of 100,000 psi failed in 87 cycles which is roughly ten times the design cycles obtained from the Code analysis. The other of these two specimens failed at 1200 cycles which is roughly equivalent to 120 times the Code design cycles.

2.7 Notched Pipe

This report includes two tests in addition to those reported in Reference (10) for notched pipe. All the calculated values (M/Z, S_p, etc.) have been corrected to be consistent with the values calculated in Reference (7).

Reference (7) gives fatigue test results on 32 straight pipe test specimens containing a machined notch. These tests are principally concerned with crack initiation and crack growth. The pertinent aspect to this report is the cycles to through-the-wall crack. The testing arrangement is shown schematically in Figure 4.

A stress concentration was provided by machining a notch, transverse to the pipe axis, about 6 inches from the flanged end. The notch was made either on the outside or inside of the pipe, as identified in Table 7 by -I (outside) or -II (inside). Details of the notch are shown in Figure 5. The theoretical stress concentration factor of the notch was 3.62. Miniature strain gages were installed on a specimen, from which the ratio of axial strain in the notch to nominal axial strain was found to be 3.6 to 3.7, in good agreement with the theoretical concentration factor.

The notched pipe tests involved three material types (A-106-B, A-312 Type 304, and A-355 Grade P22), two test temperatures (room temperature and 550 F), and various internal pressures. The elevated temperature tests were conducted without internal pressure with one exception. Test HSNP-1-II was conducted at 550 F with 1000 psig internal pressure. The room temperature tests were conducted with internal pressures of 1050 psig with two exceptions.

---

* Piping Code in use around 1949.

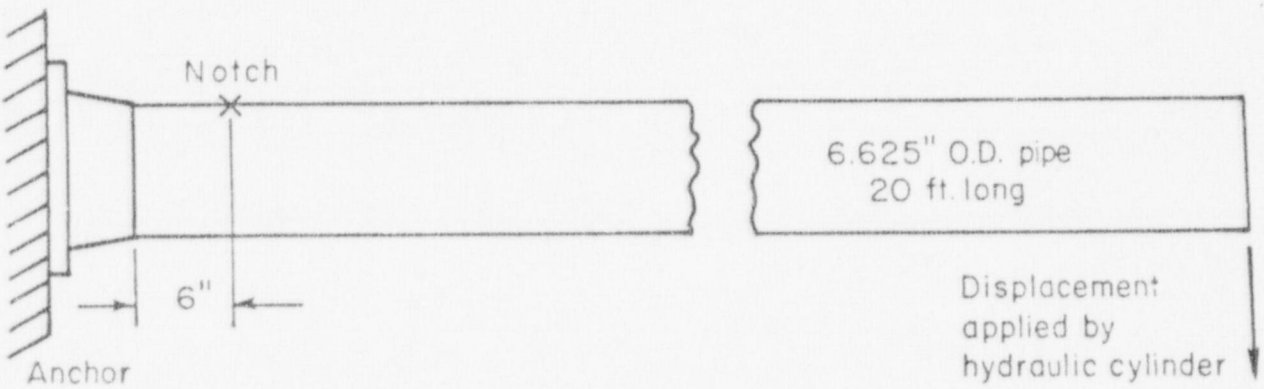

FIGURE 4. REFERENCE (7) FATIGUE TESTS OF NOTCHED PIPE

TABLE 7. EVALUATION OF TESTS ON 6-INCH NOTCHED PIPE WITH A THEORETICAL STRESS CONCENTRATION FACTOR OF 3.6, MOMENT LOADING

Specimen Number[1]	Material and Schedule[2]	M/Z, ksi	$\frac{S_n}{3S_m}$	S_p, ksi	S_{alt}, ksi	K_e	N_c	N_t	N_t/N_c
CSS-3-I	C.S., 40	80.1	1.338	288.5	242	1.676	66	1,085	16.5
CSS-4-II	C.S., 40	67.6	1.129	243.5	154	1.258	200	4,572	22.8
CSS-5-I	C.S., 40	54.1	0.901	195.0	98	1.0	640	13,398	21.0
CSS-6-II	C.S., 40	77.0	1.285	277	216	1.560	90	1,453	16.1
CSS-7-I	C.S., 80	90.5	1.510	326	330	2.020	34	1,302	35.4
CSS-8-II	C.S., 80	53.5	0.894	192.5	96	1.0	690	12,081	17.5
CSS-9-I	C.S., 80	45.3	0.726	163	82	1.0	1050	34,426	32.8
CSS-10-II	C.S., 80	44.0	0.735	158.5	79	1.0	1150	15,000	13
CSS-107-I	C.S., 80	81.6	1.363	294	254	1.726	60	3,575	59.6
CSS-109-I	C.S., 80	80.1	1.338	288.5	242	1.676	66	4,000	60.7
CSS-11-I	C.S., 160	118.6	1.980	427	632	2.960	<10	953	>95
CSS-13-I	C.S., 160	67.1	1.120	242	150	1.240	210	13,600	64.8
CSS-111-I[3]	C.S., 160	97.9	1.632	352	398	2.264	22	5,150	234
HCN-1-I	C.S., 40	55.6	1.032	200	106	1.064	520	19,998	38.4
HCN-2-I	C.S., 40	69.2	1.283	249	195	1.566	110	6,520	59.3
HCN-3-I	C.S., 40	48.0	0.890	173	86	1.0	940	45,237	48.2
HCN-4-I	C.S., 40	78.5	1.456	282	268	1.902	50	3,800	76.0
CSS-15-I	S.S., 40	52.7	0.880	190	95	1.0	700	20,127	28.8
CSS-16-II	S.S., 80	60.5	1.010	218	113	1.033	440	8,596	19.5
CSS-119-I	S.S., 80	85.4	1.425	307	370	2.415	34	4,656	137

TABLE 7. (Continued)

Specimen Number(1)	Material and Schedule(2)	M/Z, ksi	$\frac{S_n}{3S_m}$	S_p, ksi	S_{alt}, ksi	K_e	N_c	N_t	N_t/N_c
CSS-23-I	S.S., 160	105.2	1.758	379	630	3.33	10	1,735	175
CSS-25-I	S.S., 160	77.5	1.292	279	276	1.973	70	11,883	170
CSS-124-I(3)	S.S., 160	77.5	1.292	279	276	1.973	70	15,119	217
HSN-5-I	S.S., 40	56.6	1.050	204	119	1.167	740	4,701	6.3
HSN-1-I	S.S., 40	61.0	1.131	220	158	1.436	320	4,350	13.6
HSNP-1-II	S.S., 80	68.2	1.265	246	224	1.820	120	4,900	40.8
CSS-27-I	A.S., 40	81.2	1.355	292	354	2.420	27	1,500	55.6
CSS-29-I	A.S., 40	55.6	0.929	200	100	1.0	600	11,950	19.9
CSS-31-I	A.S., 80	88.5	1.478	318	463	2.910	15	4,800	320
CSS-35-I	A.S., 160	55.6	0.929	200	100	1.0	600	40,000	68.3
CSS-36-II	A.S., 160	54.0	0.901	194	97	1.0	660	19,000	30.3
CSS-37-I	A.S., 160	113.5	1.895	409	463	4.580	15	2,365	158

(1) Specimens with first identification letter C were run at room temperature; H at 550 F. Most room temperature tests were run with 1050 psi internal pressure. All 550 F tests were run at zero internal pressure, except HSNP-1-II, for which the internal pressure was 1000 psi. -1 indicates outside notch, -II indicates inside notch.

(2) Material identification:

C.S. = A-106 Grade B carbon steel
S.S. = A-312 Type 304 stainless steel
A.S. = A-355 Grade P22, 2-1/4 Cr - 1 Mo steel.

(3) Specimens tested at constant PWR pressure of 2200 psi.

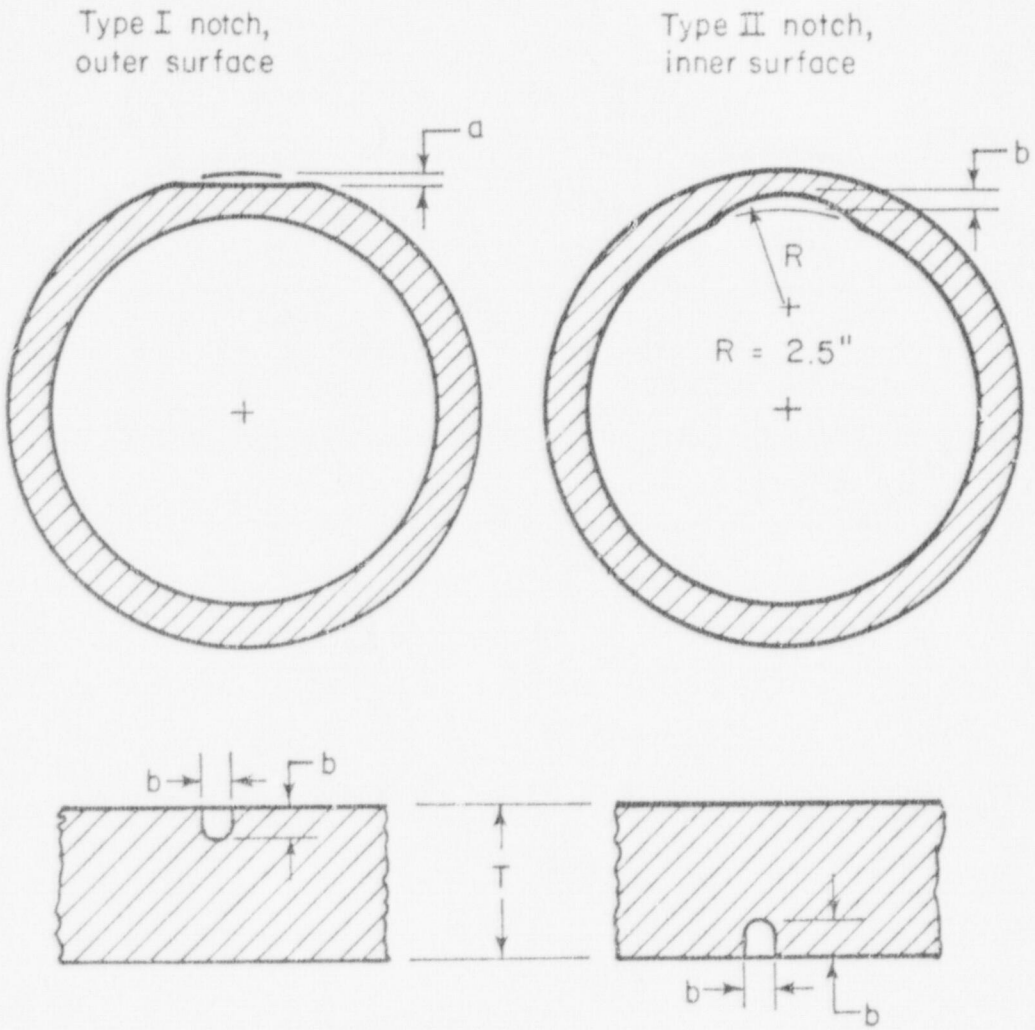

b = 0.16T

T = pipe wall thickness
= 0.280 (Sch 40), 0.432 (Sch 80), 0.718 (Sch 160)

FIGURE 5. DETAILS OF NOTCH USED IN REFERENCE (7) NOTCHED PIPE TESTS

Tests CSS-111-I and CSS-124-I were conducted with internal pressures of 2200 psig.

The loading for the notched pipe tests was provided by a controlled displacement of the end of the test pipe. It should be noted that as cracks initiated and grew from the notches the effective stiffness of the pipe decreased resulting in a changing stress state at the crack. This changing stress state is characteristic of constant amplitude deflection controlled tests.

There are, of course, no stress indices for "notches" given in the Code. However, following the spirit of the Code, a C_2-index of unity and a K_2-index of 3.6 would be assigned on the assumption that stresses due to the notch were highly localized. The evaluation of these data follows the same general procedure used previously.

The last column of Table 7 gives ratios of test cycles N_t to design cycles, N_c. These vary from 6.3 to 320; the overall average of N_t/N_c is 74.1. In general, these results indicate satisfactory conservatism of the Code evaluation method. The values of N_t shown in Table 7 are the number of full-range cycles applied to produce a crack through-the-wall. In addition, subsequent to crack initiation, a variable number of cycles of less-than-full-range were applied; these were probably of the order of one-half of the full range.

2.8 Pressurized Vessels

This section is essentially the same as the "Pressure Loading" section of Phase Report Number 115-10.[10] The information is included here because these vessels are perhaps a closer representation of the cold leg piping than any of the small-scale components. The nozzles discussed in this section represent a type of fabricated tee. In most cases, the analysis was carried out as if the Code reinforcement requirements were met.

Data from cyclic pressure tests on nozzles in cylindrical pressure vessels, and one set of cyclic pressure test data on longitudinal welds in cylindrical pressure vessels are discussed in this section. The latter were an unintended but informative by-product of tests on nozzles in the vessels.

The evaluation of these tests involve the first term of Equations (1) and (2); these are:

$$S_n = C_1 \frac{P_o D_o}{2t} \tag{6}$$

$$S_p = C_1 K_1 \frac{P_o D_o}{2t} \tag{7}$$

2.8.1 Nozzles in Pressure Vessels-I. Pickett and Grigory[19] give results of cyclic pressure tests on a series of eight cylindrical pressure vessels containing various types of nozzles. The cylinders were 40-inch O.D. x 2-inch-wall-thickness. The vessel material is indicated in Table 8 along with pertinent parameters for comparison of the test data with the Code design procedure.

In these tests, pressure was cycled from zero to the maximum pressure shown in Table 8. The corresponding maximum hoop stress is shown in the fourth column of Table 8. The hoop stress is, of course, a primary stress and is limited by the Code to S_m; i.e., to 20,000 psi for 201-B and 2-1/4 Cr-1Mo; to 26,700 psi for A-302-B. This limit is exceeded in all these tests by factors ranging from 1.3 to 2.2.

Reference (19) tests include eight pressure vessels, six of which are listed in Table 8. The other two vessels were made of "T-1" material for which the Code does not give allowable stresses. Also, in these two vessels, only one nozzle leakage failure occurred; the other leakage failures occurred in the longitudinal seam weld of the vessel shell or in the vessel shell.

The comparisons shown in Table 8 are for failures at nozzles where the crack penetrated through-the-wall to produce leakage. The nozzles involved in these failures are identified in Reference (19) and Table 8 by the Numbers 1, 2, 6, 9B, and 11. These nozzles, as well as other nozzles, were placed in one or more of the eight vessels tested. Some comments concerning these nozzle designs are given below.

TABLE 8. EVALUATION OF CYCLIC PRESSURE FATIGUE TESTS ON NOZZLES IN PRESSURE VESSELS, TEST DATA FROM REFERENCE (19)

Vessel No.	Nozzle No.	P_o	$\frac{P_o D_o}{2t}$	S_n	$\frac{S_n}{3S_m}$	S_p, ksi	K_e	S_{alt}, ksi	N_c	Test N_t	N_t/N_c
1	11	4,325	43,250	86,500	1.44	147,000	1.88	138,000	200	5,174	26.0
(201-B)	1									7,223	36.0
	6									7,516	38.0
2	6	2,650	26,500	53,000	0.88	90,000	1.00	45,000	6,000	85,868	14.0
(201-B)	2									123,620	23.0
3	1	4,400	44,000	88,000	1.10	150,000	1.40	105,000	550	8,990	16.0
(302-B)											
4	6	3,460	34,600	69,200	0.87	117,500	1.00	58,750	2,750	40,041	15.0
(302-B)	11									48,437	18.0
7	9B(1)	2,650	26,500	53,000	0.88	90,000	1.00	45,000	(1)	23,908	(1)
201-BO	11									135,600	23.0
	2N									375,357	62.0
2-1/4 Cr-1Mo	1	4,400	44,000	88,000	1.47	150,000	2.88	216,000	85	21,070	25.0

(1) Nozzle 9B consisted of a 14.225-inch I.D. x 0.806-inch wall pipe in an 18-inch I.D. radius x 1.000-inch wall spherical head. It is essentially an unreinforced nozzle. The code does not give C_1- or K_1-indices for this kind of a branch connection.

Nozzle 1. The branch pipe was 10.75-inch O.D. by 0.593-inch-wall-thickness. Reinforcing consisted of a weld-on ring. The ring dimensions are not given in Reference (19); however, by scaling from the drawings, it appears that the nozzle has close to 100 percent area replacement reinforcement. However, this would not be an acceptable nozzle under the Code. This type of nozzle was used in Vessels 1, 3, 5, and the 2-1/4 Cr-1Mo vessel.

Nozzles 2 and 2N. The branch pipe was 10.75-inch O.D. x 0.593-inch-wall-thickness. The nozzle is of the type shown in the Code, Figure NB-3643.3(a)-1(a) with θ = 14 degrees. The reinforcement used does give 100 percent area replacement. However, because of the limit to the reinforcing zone given in the Code, the reinforcing considered as effective is only 36 percent of that required. Accordingly, this model does not meet Code requirements. Nozzles of Type 2 were used in Vessels 1 through 6 and the 2-1/4 Cr-Mo vessel. Nozzles 2 and 2N differ only in that Nozzle 2 was a "set-on" type, while Nozzle 2N was a "set-in" type.

Nozzle 6. The branch pipe was 10.75-inch O.D. x 0.593-inch-wall-thickness. The nozzle is of the type shown in the Code, Figure NB-3643.3(a)-1(c) with θ = 37 degrees. The reinforcement used is about 80 percent area replacement. Accordingly, it does not meet Code requirements. Nozzles of this type were included in all vessels except Vessel 7.

Nozzle 9B. The branch pipe was 15.84-inch O.D. x 0.806-inch-wall-thickness. This nozzle was placed in one of the heads of test vessel No. 7. The head was a spherical shell with 18-inch inside radius x 1-inch-wall-thickness. This is essentially an unreinforced branch connection in the head. The Code does not give stress indices for such nozzles.

Nozzle 11. The branch pipe was 2.375-inch O.D. x 0.1875-inch-wall-thickness. This is essentially an unreinforced nozzle. The Code permits certain small nozzles to be unreinforced; however, one of the restrictions is that

$$d \leq 0.2 \sqrt{R_m T_r} ,$$

where,

d = opening size

R_m = run pipe mean radius

T_r = thicknes of run pipe.

For this model, d = 2 inches and $0.2 \sqrt{R_m T_r} = 0.2 \sqrt{19 \times 2} = 1.23$ inches. Accordingly, d is not less than $0.2 \sqrt{R_m T_r}$ and the nozzle does not meet the requirements of the Code.

While none of the nozzles are in strict accordance with Code requirements, we will nevertheless use the C and K indices listed in the Code. They are: $C_1 = 2.0$, $K_1 = 1.7$. Table 8 shows the maximum test pressure P_o and the nominal stress $P_o D_o/2t$. Because the pressure was cycled from 0 to P_o, the secondary stress range is $C_1 P_o D_o/2t$, or simply twice the nominal stress. The peak stress range is 1.7 times the secondary stress range. Three tests where $S_n < 3S_m$ are also included in Table 7 for general interest.

The last column of Table 8 shows that the value of N_t/N_c is always greater than 14 despite the significant violation of primary stress limits and branch connections which do not fully meet Code requirements.

2.8.2 Nozzles in Pressure Vessels-II. Kameoka, et al.,[20] give results of tests on the six nozzles in cylindrical vessels listed in Table 9. Nozzle Types[a] T13 and T*13 failed in the longitudinal seam in the vessel; these will be discussed later. Results for nozzle Types F13, F*13, T20, and F20 are summarized in Table 10.

The Code requires 100 percent area replacement for these nozzles. The approximate percentage of area replacement is:

(a) These are identifications used in Reference (20).

TABLE 9. DIMENSIONS AND MATERIAL DATA, REFERENCE (20)
NOZZLES IN CYLINDRICAL VESSELS

Nozzle Type	Vessel D in.	Vessel T in.	D/T	d_i/D	t/T	Nozzles r_o/T	r_i/T	δ/T
T13	11.63	0.512	22.7	0.152	0.815	1.82	0.231	0.915
F13	11.63	0.512	22.7	0.152	1.00	0.5	0.315	-0-
T*13	11.63	0.512	22.7	0.233	1.815	1.82	0.231	0.915
F*13	11.63	0.512	22.7	0.233	1.00	0.5	0.314	-0-
T20	11.60	0.788	14.7	0.233	1.04	0.435	0.33	-0-
F20	11.60	0.788	14.7	0.233	1.04	0.435	0.33	-0-

	Chemical Analysis (%)								
Material	C	Si	Mn	P	S	Ni	Cr	Mo	V
ASTM A302B	0.20	0.42	1.15	0.016	0.10	0.65	0.38	0.50	--
JIS. SF60	0.40	0.28	0.68	0.012	0.022	--	--	--	--
FTW60	0.17	0.27	1.18	0.014	0.011	--	--	--	0.072

	Tensile Test Data (Average as Tested)			
Material	Yield, psi	U.T.S., psi	Elong. %	Red. in Area, %
ASTM A302B	72,000	94,000	26.0	62.0
JIS. SF60	51,200	86,700	26.0	35.0
FTW 60	89,600	99,600	32.0	69.0

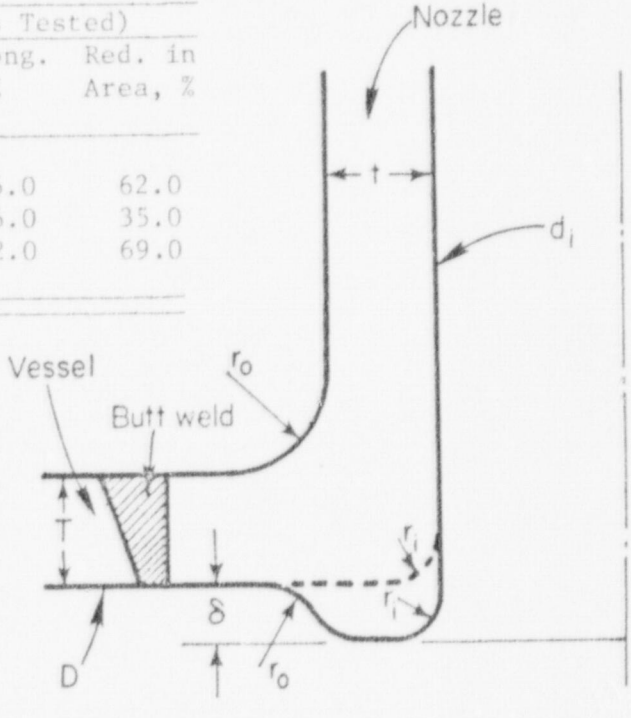

TABLE 10. EVALUATION OF CYCLIC PRESSURE TESTS ON NOZZLES IN CYLINDRICAL PRESSURE VESSELS, DATA FROM REFERENCE (20)

Nozzle No.	P_o	$\frac{P_o D_o}{2t}$	S_n	$\frac{S_n}{3S_m}$	S_p	K_e	S_{alt}, ksi	N_c	Test N_t	N_t/N_c
F13-F	5,400	64,100	128,200	1.61	218,000	3.44	375,000	24	6,518	272.0
-D	5,120	60,700	121,400	1.52	206,000	3.08	317,000	38	7,553	198.0
-C	4,835	57,300	114,600	1.43	195,000	2.72	265,000	55	9,772	177.0
-B	4,270	50,600	101,200	1.265	172,000	2.06	177,000	140	15,553	111.0
F*13-1	7,110	84,300	168,600	2.11	287,000	5.00	718,000	<10	2,781	>278.0
-4	5,690	67,500	135,000	1.69	229,000	3.76	430,000	10	8,586	859.0
-2	5,120	60,700	121,400	1.52	206,000	3.08	317,000	37	14,805	400.0
-3	4,270	50,600	101,200	1.265	172,000	2.06	177,000	140	20,505	146.0
T20-D	7,820	61,400	122,800	1.53	208,700	3.12	326,000	35	4,376	125.0
-A	6,830	53,600	107,200	1.34	182,000	2.36	215,000	90	6,145	68.0
-C	6,260	49,000	98,000	1.23	166,600	1.92	160,000	190	9,455	50.0
-B	5,690	44,600	89,200	1.12	151,600	1.48	112,000	500	19,032	38.0
F20-E	7,100	55,900	111,800	1.40	190,100	2.60	247,000	65	3,462	53.0
-F	6,260	49,100	98,200	1.23	166,900	1.92	160,000	190	6,398	34.0
-A	5,690	44,600	89,200	1.12	151,600	1.48	112,000	500	14,288	29.0
-C	4,835	38,000	76,000	0.95	129,200	1.00	64,500	2000	20,890	10.4

$S_n = 2(P_o D_o/2t)$, $S_p = 3.4(P_o D_o/2t)$, S_m = 26,700 psi (ASTM A-302-B).

Nozzle Type	Percent of Area Replacement	
T13	145.	Failure in longitudinal
T*13	094.	butt weld
F13	052.	
F*13	035.	Failure at inside corner
T20	067.	of nozzle
F20	050.	

Accordingly, none of the nozzles listed in Table 10 meet Code requirements. However, the evaluation is based on $C_1 = 2.0$, $K_1 = 1.7$; i.e., the Code indices for branch connections per NB-3643.

The material used for the nozzles was either ASTM A-302-B or JIS.SF60; the reference does not indicate which nozzle was made from which material. The evaluation is based on ASTM A-302-B, $S_m = 26,700$ psi, $m = 2.0$, $n = 0.2$ (low-alloy steel).

The data in Table 10 is analogous to that of Table 8. The tabulated values under $P_o D_o/2t$ show that the membrane stress was higher than the primary stress limit of $S_m = 26,700$ psi. Despite the violation of the primary stress limit and nozzles which did not fully meet requirements, the value of N_t/N_c in Table 10 is always greater than 10.

It can be seen in Table 10 that there is a consistent relationship between $S_n/3S_m$ and N_t/N_c within any one type of nozzle. This suggests that the K_e-factor may be over-compensating for the effect of plastic straining.

Table 11 lists four cyclic pressure fatigue tests on nozzles. In each case, the nozzles were considered to be without reinforcement. For this reason, the reduced thickness value was calculated (as in Section 2.5). As may be noted from Table 11, the N_t/N_c values range from 98.8 to 403. Clearly, the use of the reduced thickness in the Code analysis results in conservative results. The K_e factor may be responsible for the very large values of N_t/N_c in this group of tests but it would be difficult to separate the K_e influence from the reduced thickness influence. Therefore, suffice it to note that the use of the reduced thickness calculation and the correction for stress intensities above $3S_m$ results in a very conservative analysis.

TABLE 11. EVALUATION OF CYCLIC PRESSURE TESTS ON NOZZLES IN CYLINDRICAL PRESSURE VESSELS, DATA FROM REFERENCES 27 AND 28

Ref. No.	P_o, psi	$\frac{P_o D_o}{2t}$, ksi	S_n, ksi	$\frac{S_n}{3S_m}$	S_p, ksi	K_e	S_{alt}, ksi	N_c	Test N_t	N_t/N_c
(27) Nozzle 1*	1,566	44.9	89.1	1.286	152.8	2.145	163.9	180	29,200	162.0
(28) Pressure Vessel #1*	1,707	41.9	83.9	1.2	142.6	1.8	128.3	250	24,700	98.8
(28) Pressure Vessel #2*	2,134	52.5	104.9	1.5	178.3	3.00	267.4	55	22,200	403
(28) Pressure Vessel #3*	1,565	45.5	91.0	1.3	154.6	2.21	170.5	150	33,000	220

* Calculations based on reduced thickness T_r, see text.

Note: Material for all vessels was A336.

2.8.3 Longitudinal Butt Welds in Pressure Vessels. As noted in the preceding discussions of the results by Kameoka, et al.,[20], vessels with nozzle Types T13 and T*13 did not fail in the nozzles but in the longitudinal butt welds. There are a number of other literature references (including Reference (19), in which longitudinal weld failures have occurred prior to failure of a nozzle in a vessel undergoing a cyclic pressure test.

The Code gives stress indices for longitudinal butt welds in straight pipe. For Class I piping with surfaces "as welded", these are: $C_1 = 1.1$, $K_1 = 1.2$. However, there is an important restriction to the K_1-index; i.e., it is only applicable to pipe with a circular cross section. Unfortunately, Reference (20) does not give any significant details as to the longitudinal butt welds or the out-of-roundness of the vessel. Table 12 gives an evaluation of the tests under three separate assumptions:

(1) The vessel cross section was circular, $C_1 = 1.1$, $K_1 = 1.2$

(2) The vessel cross section was out-of-round such that $D_{max} - D_{min} = 0.5t$. The equation shown in Table NB-3682.2-1 of the Code was used to determine the additional stress due to out-of-roundness. The value of C_1 is still 1.1, but

$$K_1 = 1.2 \left\{ 1 + \frac{D_{max} - D_{min}}{t} \left[\frac{1.5}{1 + 0.455 \left(\frac{D_o}{t} \right)^3 \frac{P_o}{E}} \right] \right\} \qquad (8)$$

The modulus of elasticity, E, was taken as 3×10^7 and $D_o/t = 22.7$ for the vessels, from which

$$K_1 = 1.2 + \frac{0.9}{1 + 0.000177\ P_o}$$

(3) The vessel cross section was out-of-round such that $D_{max} - D_{min} \leq 0.08\ D_o$. The equation shown in footnote (1.C), Table NB-3682.2-1 of the Code was used to determine the peak stress due

TABLE 12. EVALUATION OF CYCLIC PRESSURE TESTS ON LONGITUDINAL BUTT WELDS IN CYLINDRICAL PRESSURE VESSELS, DATA FROM REFERENCE (20)

Model No.	P_o	$\frac{P_o D_o}{2t}$	S_n	$\frac{S_n}{3S_m}$	K_e	Test N_t	Assumed Cross Section[a]	S_p	$\frac{K_e S_p}{2}$	N_c	N_t/N_c
T-13-F	6,260	77,600	85,400	1.07	1.28	5,982	Circle	102,400	65,500	1,900	3.1
							Ellipse	139,000	89,000	850	7.0
							Limit	486,000	312,000	38	157.0
-D	5,500	68,800	75,700	0.95	1.00	9,102	Circle	90,800	45,400	6,000	1.5
							Ellipse	125,000	62,500	2,100	4.3
							Limit	431,000	215,000	90	101.0
-C	5,120	63,500	69,800	0.87	1.00	28,286	Circle	83,800	41,900	7,500	3.8
							Ellipse	117,000	58,500	2,750	10.3
							Limit	398,000	199,000	105	269.0
T*13-4	7,100	88,200	97,000	1.21	1.84	4,360	Circle	116,400	107,700	550	7.9
							Ellipse	155,000	143,000	240	18.2
							Limit	552,000	508,000	13	335.0
-2	5,690	70,500	77,600	0.97	1.00	9,502	Circle	93,100	46,600	5,000	1.9
							Ellipse	128,000	64,000	2,000	4.5
							Limit	443,000	221,000	85	112.0
-3	5,000	61,700	67,900	0.85	1.00	9,116	Circle	81,400	40,700	7,500	1.2
							Ellipse	114,000	57,000	3,000	3.0
							Limit	386,000	193,000	115	79.0
-1	4,270	52,900	58,200	0.73	1.00	21,135	Circle	69,800	34,900	13,000	1.6
							Ellipse	99,600	49,800	4,500	4.7
							Limit	332,000	166,000	160	132.0

[a] For elliptical cross section, $D_{max} - D_{min} = 0.5t$.

to out-of-roundness. The C_1 value remains unchanged but the K_1 value is computed by

$$K_1 = (K_1)_{round} \left[1 + \frac{MS_y}{PD_o/2t} \right] , \qquad (9)$$

where

M = 2.0 for ferritic steels and nonferrous materials except nickel-chrome-iron alloys and nickel-iron-chrom alloys

M = 2.7 for austentic steels, nickel-chromium-iron and nickel-iron-chromium alloys

S_y = yield strength at design temperature, psi

P = design pressure

Assuming $PD_o/2t = S_m$, then for A-302-B at room temperature:

$$K_1 = 1.2 \left[\frac{2 \times 50,000}{26,700} \right] = 5.7 .$$

The material used in the vessel shells (FTW 60) had tensile properties similar to ASTM A-302-B; hence, the values of S_m, S_y, m, and n for A-302-B were used in the evaluation shown in Table 12.

The last column of Table 12 shows N_t/N_c values approaching unity if the vessels were actually round and had high-quality welds. However, even a small amount of assumed out-of-roundness brings N_t/N_c up significantly. The vessels were apparently formed in halves with two longitudinal butt welds. The abutting plate edges, particularly in experimental models, often are not rolled to the same radius as the body of the plate, leaving either a "peak" or a "flat spot" at the weld. For a given amount of out-of-roundness, these kinds of local irregularities give higher stresses than indicated by Equation (8) which is for an elliptical out-of-round shape. The "limit" analysis is applicable to any cross section shape (up to an out-of-roundness of 0.08 D_o, which the model vessel shells presumably met) and, as shown in Table 12, this analysis gives N_t/N_c values well above 20.

The purpose of including the data on longitudinal butt welds is to point out that such welds, in conjunction with out-of-roundness, can be a significant source of high stresses; a source recognized in the Code. However, to bring the test results into perspective, it should be noted that the lowest number of cycles was 4360; this for a pressure range of zero to 7100 psi. The design pressure for this vessel (of A-302-B, S_m = 26,700 psi) is about 2300 psi.

2.9 Thermal Gradient Loading

This report includes no test results in addition to those reported in Phase Report Number 115-10[10] for thermal gradient loading. This section is the same as the section in Report 115-10 and is included here for the sake of completeness.

The third type of loading considered by the Code is that arising from thermal gradients. While a fair number of thermal fatigue tests on bar specimens are available in the literature, very little has been done on thermal cycling tests of piping components. Stewart and Schreitz[22] give results of thermal shock tests on 6-inch Schedule 80 and Schedule 160 pipe and valves therein. Weisberg and Soldan[23] give results of tests on pipe and girth butt welds therein as do Tidball and Shrut[24] and Gysel, Werner, and Gut[25]. These tests and results are not in sufficiently quantitative form to permit meaningful comparisons with the Code fatigue approach. Further, these tests involve temperatures above that covered by the Code and therefore were not included in this study.

The writer obtained (from a source that cannot be referenced at this time) results of thermal gradient tests which are pertinent to this report. These tests, their results and a Code evaluation of the results are discussed in the following.

Thermal gradient tests were conducted on a piping system made up of 1-inch Schedule 80 (1.315-inch-O.D. x 0.179-inch nominal wall) piping and tees. The material was Ni-Cr-Fe Alloy 600. The fluid entrance to the section consisted of a butt welding tee; the butt welds between it and the pipe are the "components" of interest herein.

Thermal gradients were created by circulating hot water at 595 F ± 5 F and 2900 ± 100 psi through the test section at the rate of 35 gpm, followed by circulating cold water at 70 ± 10 F and 60 ± 10 psi. A typical thermal cycle was initiated by circulating hot water through the test section for 2 minutes; the fluid temperature near the inlet increasing from 70 F to 595 F in 2 seconds. Circulation of water was then stopped and the test section was allowed to "soak" at high temperature for 1.5 minutes in order to thoroughly heat the entire test section. During this period, the fluid temperature decreased 100 F. Cold water was then circulated through the test section for 3.5 minutes; the fluid temperature near the inlet decreasing from about 470 F to 70 F in 2 seconds. The total length of time for a complete cycle was 7 minutes.

At the completion of 2206 cycles, the test section was hydrostatically tested at a pressure of 4750 psi at 80 F for 15 minutes. There was no indication of leakage. A liquid penetrant inspection of the outside surface after the hydrostatic test did not indicate any cracks. The inlet tee and girth butt welds between it and the pipe were then cut out of the test section and sectioned for internal surface inspection. The tee, flow direction, and welds are identified in the following sketch. Liquid penetrant inspection of the inside indicated a crack in the heat-affected zone of weld Number 10. Further examination of the crack indicated it was about 0.30-inch deep (17 percent of the wall thickness) and had propagated in both a transgranular and intergranular pattern. The source of the test results was of the opinion that the crack pattern could have been aused by fatigue.

In summary, after 2206 cycles of thermal gradients, girth butt weld Number 12 had no detectable cracks, girth butt weld Number 10 had a small crack, the entrance tee had no detectable cracks. It is pertinent to note that girth butt weld Number 12 would nominally undergo the highest thermal gradients; girth butt weld Number 10 very slightly lower gradients and girth butt weld Number 11, much lower thermal gradients. Details of the butt welds, or the relationship (if any) of the crack to root irregularities of weld Number 10 are not known at this time. The following Code evaluation is based on the assumption that girth butt weld Number 10 was "as-welded", as classified in the Code, Table NB3682.21.

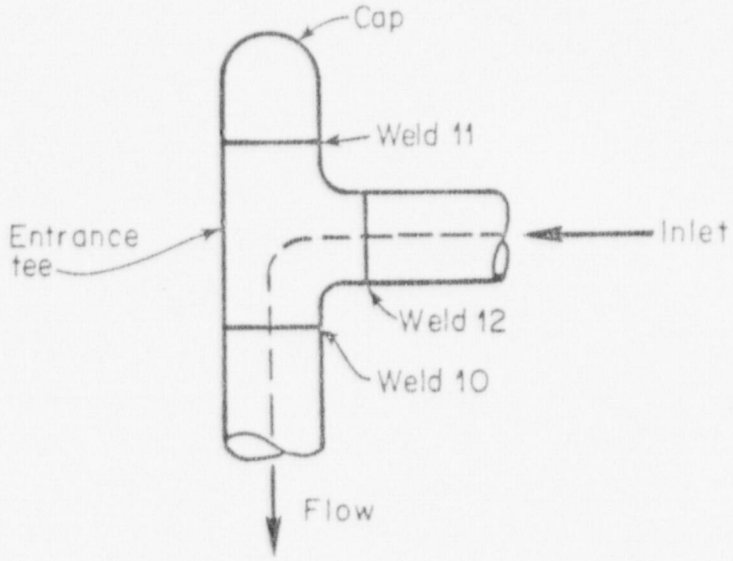

The value of S_n for the thermal gradient tests of girth butt weld Number 10 is given by

$$S_n = \frac{P_o D_o}{C_1 2t} + \frac{1}{2(1-\nu)} E\alpha\left|\Delta T_1\right| . \qquad (10)$$

The M_i term is not included in Equation (10) on the assumption that the test section was supported so that it was free to expand. The value of S_p is given by

$$S_p = K_1 C_1 \frac{P_o D_o}{2t} + \frac{K_3}{2(1-\nu)} E\alpha\left|\Delta T_1\right| + \frac{1}{1-\nu} E\alpha\left|\Delta T_2\right| . \qquad (11)$$

In the above equations

$C_1 = 1.1$
$K_1 = 1.2$
$K_3 = 1.7$

Per Table NB-3682.2-1 "as welded" girth butt weld

P_o = pressure range = 2900 - 60 = 2840 psi

D_o = pipe O.D. = 1.315 in.

t = pipe nominal wall thickness = 0.179 in.

ν = Poisson's ratio = 0.3

$E\alpha$ = modulus times coefficient of thermal expansion (= 226 for Ni-Cr-Fe Alloy 600 at 70 F).

The procedure for obtaining ΔT_1 and ΔT_2 is given in the Code. The data given by Schneider[26] will be used as being sufficiently accurate. Specifically, for a step change in fluid temperature, Schneider's Chart 23 was used. This chart gives the temperature response of a plate insulated on one side after sudden exposure to a uniform temperature convective environment on the opposite side. The chart is given in terms of the parameters:

$$Bi = h\delta/K$$

$$Fo = \alpha_d \theta/\delta^2$$

where,

h = film coefficient, Btu/hr-ft^2- F

δ = plate thickness, ft

K = thermal conductivity of plate material, Btu/hr-ft - F

α_d = thermal diffusivity of plate material, ft^2/hr

θ = time, hrs.

For the 1-inch Schedule 40 pipe, δ = 0.179/12 = 0.0149 ft, K = ~ 0.15. For the heat-up side of the cycle, the flow rate of 35 gpm leads to a value of h of about 2500 Btu/hr-ft^2 - F. Accordingly: Bi = 4.13. Schneider's Chart 23 then can be used to construct the temperature variation through the wall of the pipe as shown Figure 6. Values of ΔT_1 and ΔT_2 can be calculated from Figure 6 by use of the equations:

$$\bar{T} = \frac{1}{t} \int_{-t/2}^{t/2} T(y)dy \quad , \qquad (12)$$

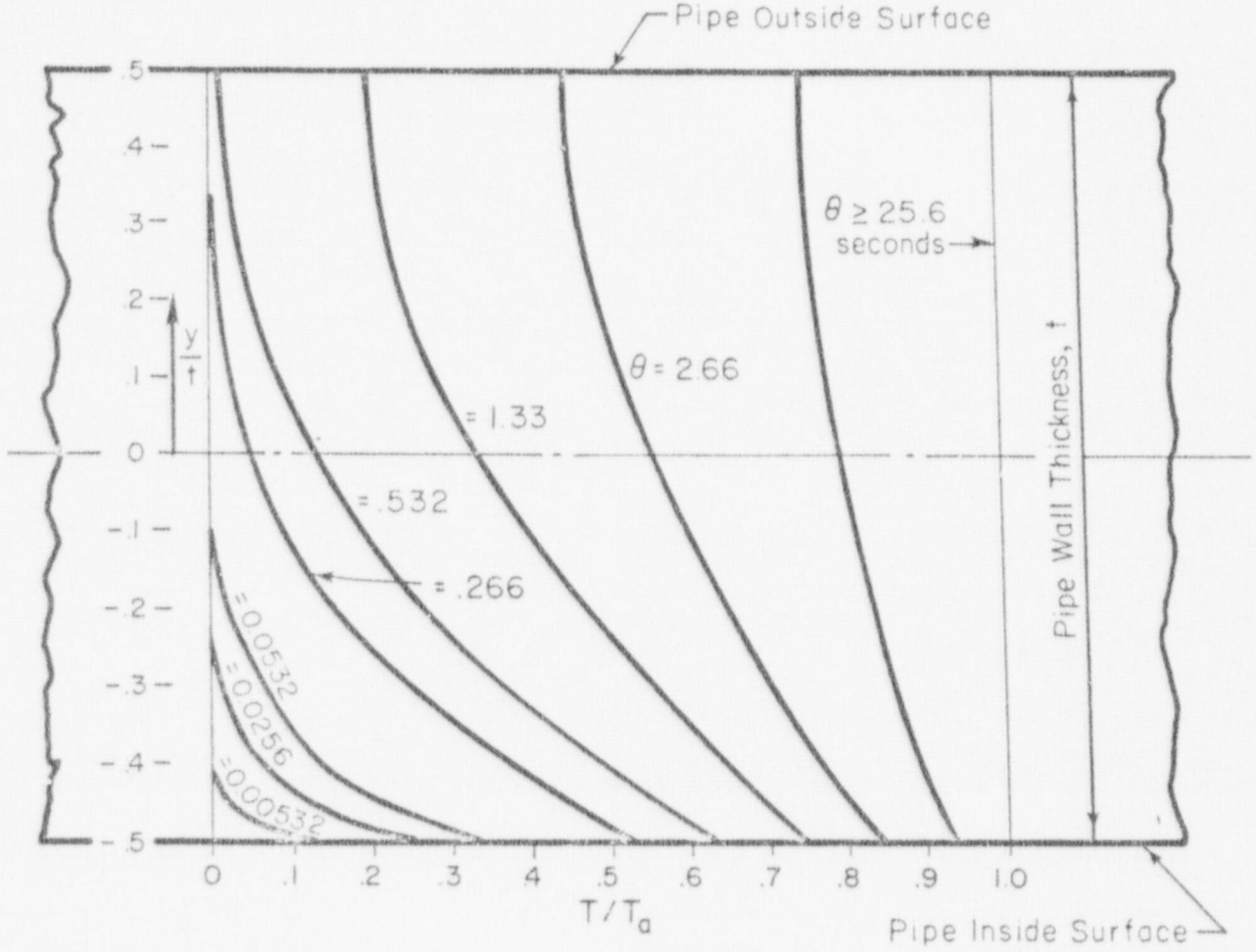

FIGURE 6. CALCULATED TEMPERATURE DISTRIBUTION THRU-WALL DURING HEATING PHASE, T_a = STEP CHANGE OF FLUID TEMPERATURE, F[26]

$$\Delta T_1 = \frac{12}{t^2} \int_{-t/2}^{t/2} y\, T(y)dy \quad , \tag{13}$$

$$\Delta T_2 = \text{Max} \left(\left| T_o - \bar{T} \right| - \left| \Delta T_1 \right| /2, \left| T_1 - \bar{T} \right| - \left| \Delta T_1 \right| /2, 0 \right) \quad , \tag{14}$$

where T_o = outside surface temperature, F; T_i = inside surface temperature, F. Numerical integration was used to evaluate Equations (23) and (24); the results are shown in Figure 7 where ΔT_1 and ΔT_2 are plotted against time, θ. The maximum during the heat-up side of the cycle are $T_1 = \sim 0.62\ T_a$, $\Delta T_2 = \sim 0.23\ T_a$.

Analysis of the cool-down side of the cycle would give graphs similar to Figures 6 and 7; with the sign of T_a reversed. The range of ΔT_1 and ΔT_2 during the cycle would be $0.23\ T_a$ and $0.62\ T_a$, where T_a is the sum of the step change in fluid temperature on the heat-up side of the cycle plus the step change on the cool-down side of the cycle. Nominally, T_a is equal to 2(595-70) = 1050 F. However, the "soak" period reduced the cool-down step change by 100 F, and other effects may have reduced the effective T_a by another 100 F. Accordingly, an estimate of T_a = 800 F will be used; $\left| \Delta T_1 \right|$ = 0.62 x 800 = 496 F, and $\left| \Delta T_2 \right|$ = 0.23 x 800 = 184 F.

Equations (10) and (11) give

$$S_n = 1.1 \times \frac{2840 \times 1.315}{2 \times 0.179} + \frac{1}{1.4} \times 226 \times 496$$

$$= 11,475 + 80,070 = 91,545 \text{ psi},$$

$$S_p = 1.2 \times 1.1 \times \frac{2840 \times 1.315}{2 \times 0.179} + \frac{1.7}{1.4} \times 226 \times 496 + \frac{1}{0.7} \times 226 \times 184$$

$$= 13,770 + 136,110 + 59,400 = 209,280 \text{ psi}.$$

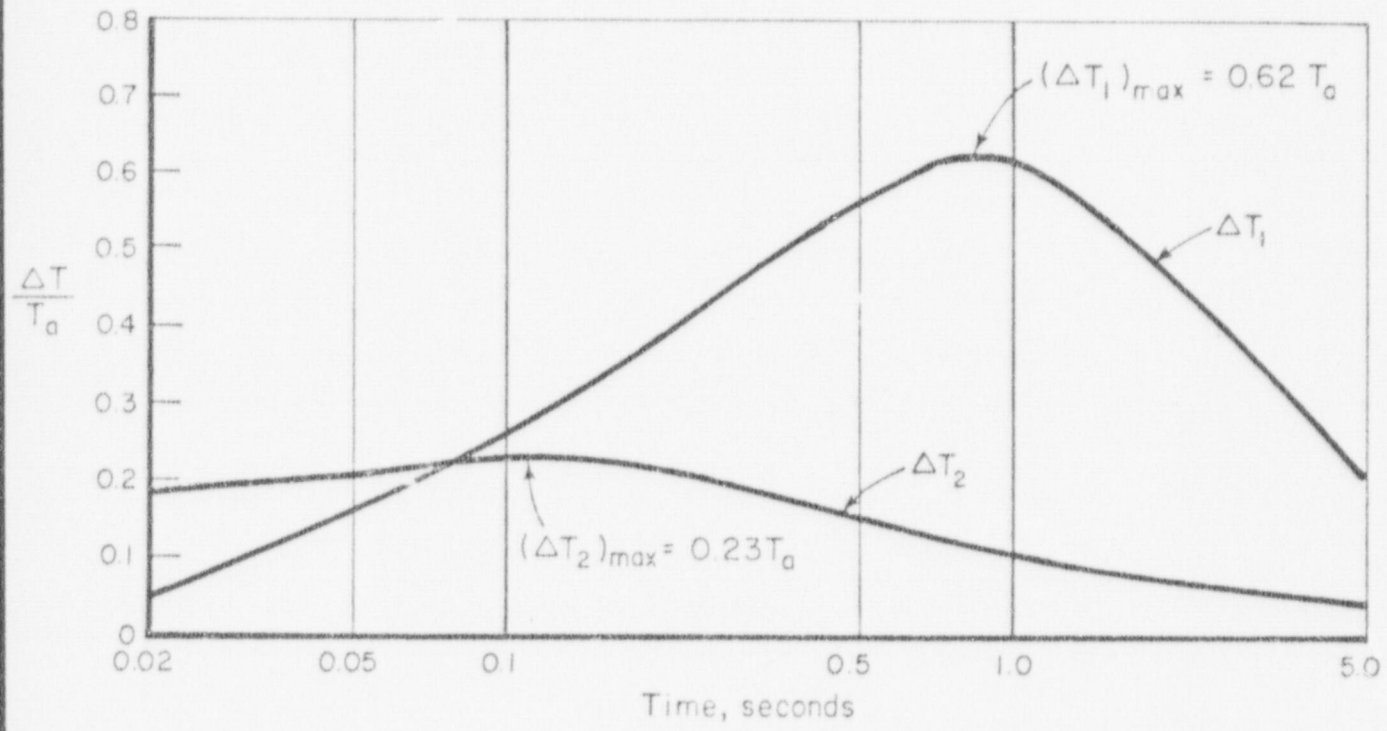

FIGURE 7. CALCULATED ΔT_1 AND ΔT_2, HEATING PHASE, T_a = STEP CHANGE OF FLUID TEMPERATURE, F[26]

For Ni-Cr-Fe alloy 600 (SB163, annealed) at 600 F, S_m = 23,300 psi. The value of K_e, by Equation (4) herein,* is

$$K_e = 1 + 3.33 \left[\frac{91,545}{3 \times 23,300} \right] - 1 \quad ,$$

and, by Equation (3)

$$S_{alt} = \frac{2.032 \times 209,280}{2} = 212,630 \text{ psi.}$$

From Figure 3, the calculated cycles, N_c, is 140. The ratio $N_t/N_c \geq 2200/140 = 16$. Accordingly, the indices method is conservative as compared to this single set of test data on thermal gradient loading; particularly considering that girth butt weld Number 10 had a crack depth of only 17 percent of the wall thickness, and girth-butt weld Number 12 had no crack indications after 2200 thermal gradient cycles.

It is of some interest to note that if K_e were to be taken as unity, the S_{alt} = 105,000; N_c = 1100, $N_t/N_c \geq 2200/1100 = 2.0$.

While details of the geometry of the entrance tee are not known, calculations based on some rough assumptions lead to the conclusion that the indices method would give about the same value of N_c as obtained for the girth butt weld. No cracks were found in the entrance tee after 2200 thermal gradient cycles.

2.10 Summary

In general, the comparison of Code predicted fatigue life and test life indicates that the Code method gives conservative results, where conservative is interpreted as $N_t/N_c \geq 20$.

---

* Values of m and n for Monel are the same as for austenitic stainless steel.

Girth butt welds in austenitic stainless steel pipe were noted as a possible exception to this conclusion in Phase Report Number 115-10[10]. The additional test results reported in section 2.1 of this report reject this exception. Although the analysis procedure is not as conservative for the stainless steel pipe as for the carbon steel, it does generally meet the $N_t/N_c \geq 20$ requirement. This trend is noted in Sections 2.1, 2.2, 2.3 and 2.4. The reverse trend was observed in Section 2.5 (Branch Connections and B16.9 Tees).

There was a trend noted in Phase Report Number 115-10[10], for the K_e factor to overcompensate when $S_n > 3S_m$ with cyclic internal pressure. This overcompensation was observed for the pressure vessel tests. A similiar trend may be found in examining the results of the cyclic internal pressure tests on Branch Connections and B16.9 Tees (Table 5). As noted in the table, the stainless steel test specimens all had $S_n > 3S_m$ by a factor of not less than 1.6. This observed overcompensation could account for the trend reversal noted earlier, i.e., that the analysis in Section 2.5 was more conservative for stainless steel specimens than for carbon steel specimens.

Perhaps the single most important result of this analysis is for specimen T-11 in Section 2.5. The value of $N_t/N_c = 5.2$ clearly implies a problem area in the Code analysis techniques for internal pressure loading with $S_n < 3S_m$. A testing program to assess, (1) what changes should be made in the analysis procedure, or (2) if any changes are needed, would be well advised.

No implication is intended that the test data are sufficiently broad in scope to confirm the validity of the indices method for all combinations of piping components, materials, temperatures, and loadings. Test data with combined loadings would be most helpful in assessing the Code's conservatism in these cases.

3.0 SIGNIFICANCE OF THE FAILURE MODE

The fatigue tests considered in Section 2 of this report represent an analysis of the behavior of piping components subjected to cyclic loadings. This analysis is in terms of the number of cycles imposed before a crack initiates and propagates through the wall thickness. Unfortunately, these tests do not describe the behavior of the component subsequent to wall penetration, i.e., a stable leak or a rupture.

This section presents an attempt to delineate the leak-rupture tendencies of the fatigue tests by comparing the appearance of the fracture to that of components used in 'burst' tests.

Several experimental programs have been conducted to determine the behavior of pipe and pipe components with through wall flaws. These programs involved burst characteristics (pressure and flaw geometries) of the pipe specimens.

The key results of these investigations, as related to this report, are the appearance of the fracture and the determination of critical flaw sizes for a given pressure level.

The remainder of this section deals with a brief summary of the burst test results and how these results pertain to the fatigue test results. A more thorough review of the burst test results and implications thereof may be found in Reference (29).

3.1 Failures in Straight Pipe

3.1.1 Background. The ultimate failure of straight pipe sections with flaws has been studied in considerable detail[30,31]. Two classes of flaws have been investigated, i.e., circumferential and axial.

The Battelle investigation[30] dealt with failure pressures and modes at elevated temperatures. The test procedure consisted of filling a test vessel (pipe section with end caps) with water and then heating the water to increase the internal pressure. Part-through flaws (surface flaws) and through-the-thickness flaws were examined. Although the part-through flaw is the more realistic type of defect, the results of testing through-the-thickness flaws serve to predict the behavior of surface flaws once they grow

through-the-thickness.

As surface flaws grow through the pipe wall they result in one of two types of failure, i.e., stable leak or a rupture. For a stable leak type of failure, the flaw penetrates the wall without any sudden increase in length. Figure 8 shows such a failure.

A rupture is denoted by a sudden increase in the flaw length as the wall is penetrated. This extension may continue until the flaw 'runs' the full length of the pipe or it may arrest due to changes in the load or pipe toughness. Figure 9 shows a full end-to-end rupture. Figure 10, on the other hand, depicts an arrested rupture.

As noted earlier, the arrest of propagating flaws can be due to several factors or some combination thereof. Perhaps the most important cause, for the purposes of this report, is the loss in driving force (stress). In a case where the only stresses on the component are due to internal pressure, loss of that pressure or a substantial reduction in pressure will cause the flaw to arrest.

For a test conducted at room temperature with water or oil as the pressurizing medium, it is unlikely that an end-to-end rupture (as depicted in Figure 9) will occur. This is simply due to the fact that once a flaw grows through-the-wall and the vessel begins to decompress, the decompression wave velocity is faster than the fracture speed. Thus, the pressure falls to near zero before the fracture can propagate an appreciable distance. This experimental problem may be overcome by installing a 'boot' or patch over the area where the flaw is expected to penetrate the wall, thereby maintaining internal pressure. For many 'real' piping systems, pressure would be maintained in the event that a flaw grows through-the-wall by additional flow provided from a system 'reservoir'. For example, in a nuclear power plant (PWR) the coolant in the primary system may be replaced at approximately 50 gpm thereby maintaining system pressure.

Testing at elevated temperatures with a fixed volume of water presents some interesting results. As with the low temperature testing, once the wall is penetrated the pressure begins to drop. However, for elevated temperatures the pressure does not go to zero but rather to the saturation pressure of the water for the test temperature. This pressure remains sensibly constant for the time required for the flaw to propagate along the

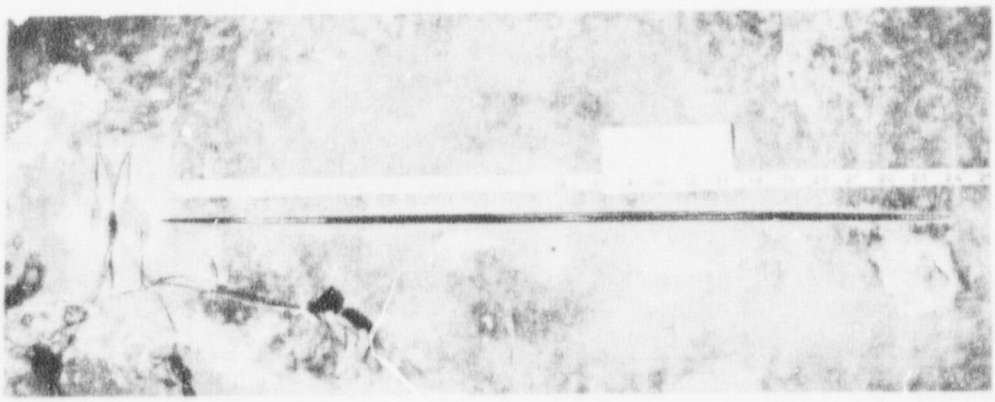

40985

FIGURE 8. LEAK IN EXPERIMENT 9 (24-INCH x 1.7-INCH A-106-B)

The pipe contained a 24.5-in. surface flaw that had a depth of 1.45-in. The saturation stress level was 8.53 ksi. Failure occurred at 584 F under a hoop stress of 8.53 ksi and a pressure of 1360 psig.

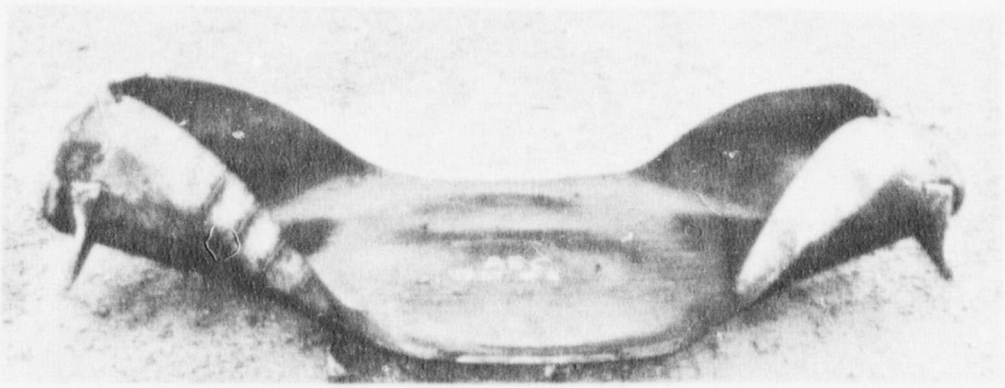

40980

FIGURE 9. FRACTURE IN EXPERIMENT 5 (24-INCH x 1.7-INCH A-106-B)

The pipe contained an 18.5-inch through-wall flaw. The saturation stress level was 16.5 ksi. Failure occurred at 675 F under a hoop stress of 16.5 ksi and a pressure of 2610 psig.

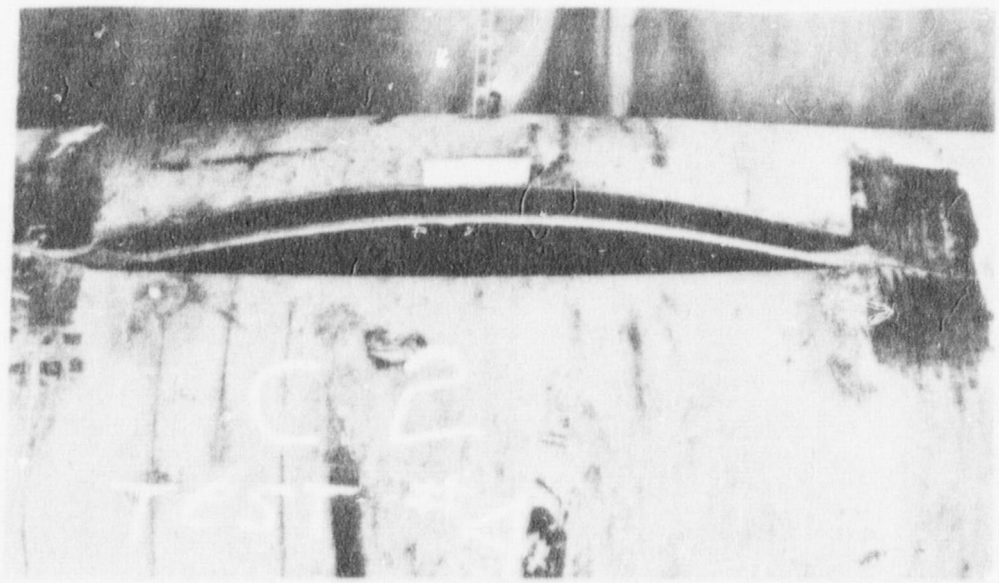

38987

FIGURE 10. FRACTURE IN EXPERIMENT 4 (24-INCH x 1.7-INCH A-106-B)

The pipe contained a 28.4-in. surface flaw that had a depth of 1.30-in. The saturation stress level was 8.96 ksi. Failure occurred at 596 F under a hoop stress of 15.1 ksi and a pressure of 2500 psig.

vessel. If the flaw is of a length critical for propagation it will start to run. If the saturation pressure is sufficient to sustain propagation an end-to-end rupture will result. If the saturation pressure is below the value required to propagate the crack it will arrest and appear as a stable leak (Figure 10).

A surface flaw will result in a rupture (assuming pressure is maintained) if its length upon penetrating the wall is the same or longer than the critical length for a through-the-wall axial crack. This critical length may be estimated by use of the K-solution developed by Maxey, et al.,[31], Equation 15.

$$K_c^2 = \frac{8\, C\, (\bar{\sigma})^2}{\pi} \ln \sec \frac{\pi M \sigma_f}{2\bar{\sigma}}, \qquad (15)$$

where,

K_c = plane strain fracture toughness

C = critical half crack length

$\bar{\sigma}$ = flow stress $\stackrel{\sim}{=} (\sigma_{yield} + 10)$ ksi

σ_f = failure stress

M = Folias correction factor given by,

$$\left(1 + 1.255 \frac{C^2}{Rt} - 0.0135 \frac{C^4}{R^2 t^2}\right)$$

t = wall thickness

R = pipe radius .

The use of this equation and the implications thereof are discussed in detail in references (32) and (33) and will not be reviewed here.

3.1.2 Experimental Results. The tests conducted by General Electric[31] involved pipe diameters ranging from 4- to 12-inches. Both through-the-wall and part-through flaws were considered. All tests were conducted at room temperature with internal seals installed for the through wall flaws. The authors noted that some of the cracks extended beyond the machined size while others did not. Because of the limited information given

in Reference 31, a detailed assessment of leak rupture behavior for these tests is not possible.

Circumferentially-oriented flaws are of particular interest. Several investigations into the behavior of circumferentially flawed pipes with internal pressure and/or bending loadings have been conducted.[31,34,35]

Some conclusions about pipe with circumferential flaws may be made based on these investigations. These are:

(1) Short flaws (0.5 d in length) have virtually no effect on the burst strength of pipe. In fact, the pipe may fail with a longitudinal fracture starting at the tip of the circumferential flaw.[31]

(2) For circumferential flaws, some type of secondary load (in this case a bending load) is needed to cause failure in the circumferential direction. For long flaws, this secondary load is a result of the nonsymmetrical cross-section and eccentric loading, at least for capped pipe sections.[35] This type of loading could also be due to external bending loads imposed on the pipe. This externally induced bending is particularly significant to piping systems. Some experimental work has been done on this effect.[31]

(3) A pipe can tolerate a substantially longer circumferential flaw than axial flaw when subjected to only a pressure loading.[36]

(4) There is some indication from one group of tests that only the long circumferential surface flaws tend to rupture.[36] There is by no means conclusive evidence that this trend is generally true although it does not seem an unreasonable result.

(5) At the present time, there is no criterion to evaluate whether a circumferential flaw will leak or rupture at failure.

In general, it may be stated that pipe, subjected to a pressure loading only, is less sensitive to circumferential flaws than to axial flaws and that there is some critical combination of flaw geometry and pressure that will result in the rupture of the pipe. From an experimental standpoint,

unless provisions have been made to maintain pressure once the wall is penetrated, the results of the test (in terms of leak or rupture) may be inconclusive.

Analytical approaches to predicting the failure pressure for circumferential flaws are not as clearly defined as for axial flaws. Some attempts have been made[38] with varying degrees of success. However, as noted earlier, a completely acceptable solution for circumferential flaws does not exist at this time.

3.2 Failure in Elbows and Tees

General Electric has conducted a series of burst tests on elbows and tees that contained surface flaws of various orientations.[36] Figure 11 shows the flaw geometries used for these tests.

Photographs of the failed specimens were included in Reference (36) and are reproduced here to illustrate the appearance of the failures. Figures 12 and 13 show the results of the elbow and tee tests, respectively.

The results of these tests can best be described by the G.E. analysis.

> "Only in those cases in which the pressure load limit was greater than 60 percent of that for an unflawed fitting did the fracture propagate beyond the ends of the original flaw. Review of the load limit data for axial part-through flaws in straight pipe segments shows that to produce a given reduction in pressure load limit, a more severe flaw is required in a tee or elbow than in a straight pipe segment. The limited number of fittings experiments done indicates that, as was the case with straight pipe segments, elbows and tees are most sensitive to flaws if the plane of the flaw is perpendicular to the maximum principal stress. In elbows, flaws of Types A and C behave much the same as axial part-through flaws of similar length in pipe segments, if corrections are made for differences in principal stress ratios at the flaw location.

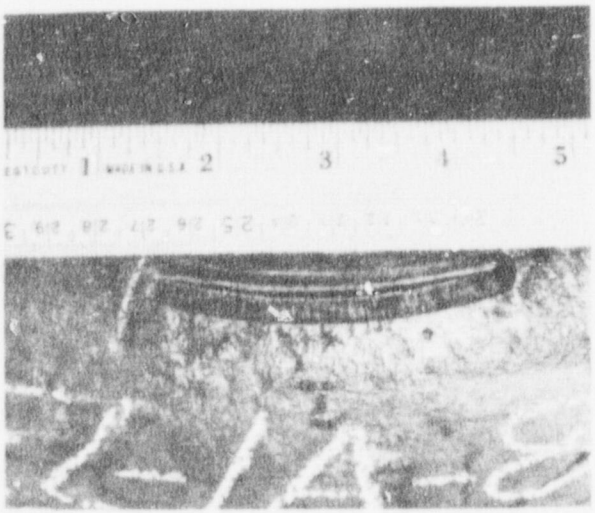

EL-1A-8

EL-2A-8

EL-3A-8

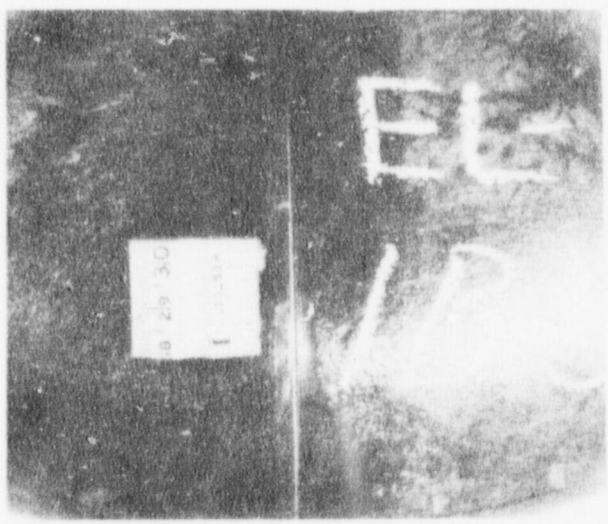

EL-1B-8

FIGURE 12. FAILURE APPEARANCES, F

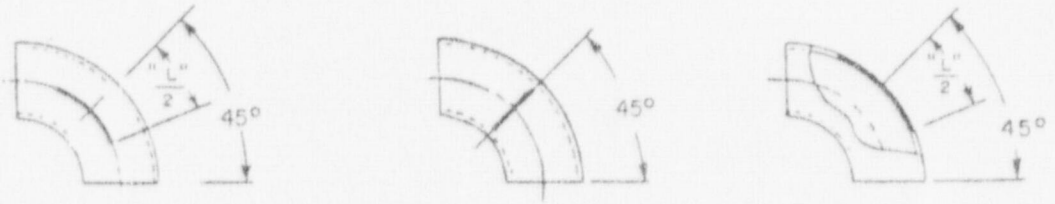

A B C

See Detail P

TYPES OF ELBOW FLAWS

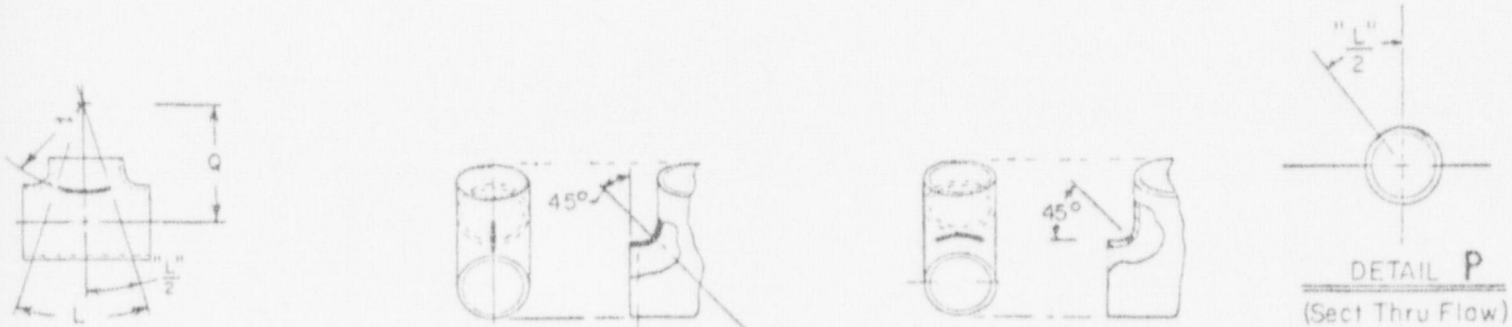

J K L

See Detail P

TYPES OF TEE FLAWS

FIGURE 11. MACHINED FLAWS IN ELBOWS AND TEES[35]

EL-2B-8

EL-1C-8

EL-2C-8

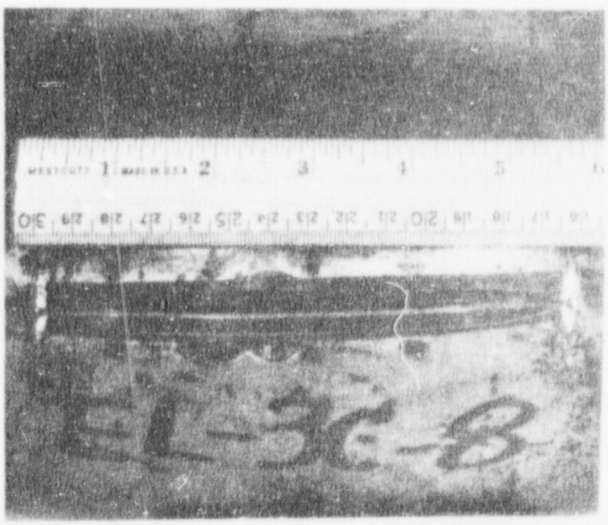

EL-3C-8

LAWED ELBOWS(35)

T-1J-8

T-2L-8

T-3L-8

FIGURE 13.

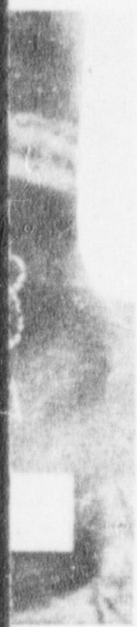

T-2J-8

T-3J-8

T-1L-8

T-1K-8

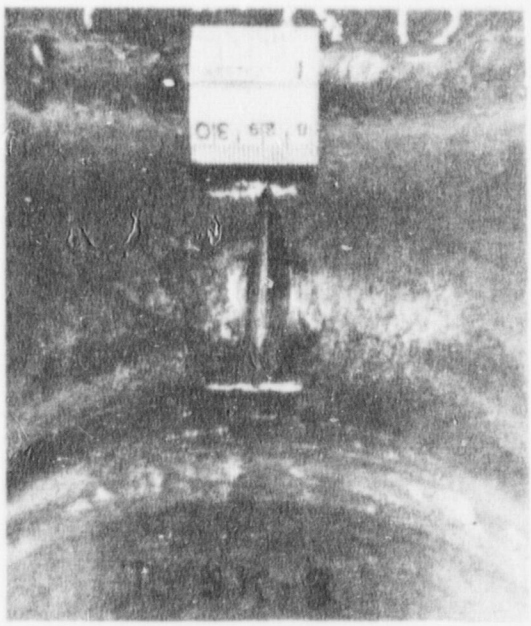

T-3K-8

FAILURE APPEARANCES, FLAWED TEES[35]

> Variations in wall thickness and stress gradients in tees render mathematical treatment of the effect of flaw size on load limit exceedingly difficult on anything more than a very rough basis. Of the three flaw configurations investigated, Types J and K cause the greatest reduction in strength when considered on a basis of flaw size (i.e., depth and length). In the absence of bending loads, tees are very insensitive to flaws of Type L."[36]

Figures 12 and 13 along with Figures 8, 9, and 10 depict the appearance of typical fractures for leak and rupture conditions. Unfortunately, the only reliable mathematical model for predicting burst pressure is for axial flaws in straight pipe.

3.3 Fatigue Fracture

Assessment of the leak rupture trends for the variety of fatigue tests tabulated in Section 2 of this report is limited by the information given in the cited references and adequate analytical techniques for the complex geometries involved.

The majority of the tests that were internally pressurized were conducted at room temperature with various liquids as the pressurizing medium (water and transformer oil were the most common). A few of the General Electric tests were internally sealed so as to prevent pressure loss once the wall was penetrated. Unfortunately, none of the elbows or tee sections were sealed.

Very few of the papers considered herein provided photographs of the failed test specimens. Only three groups of experiments provided such photographs (References 7, 13, and 15). Unfortunately, the quality of some photographs appearing in the referenced articles was such that reproduction for this report would have been worthless. Copies of some key photographs were obtained* and are included in this section. In addition, photographs of

---

* Photographs of T-4, T-6, T-11, and T-13 were provided by S. E. Moore of Oak Ridge National Laboratories. His assistance in this matter is greatly appreciated.

some of the General Electric test components are also included. The remainder of this section describes the appearance of the failed test components and attempts to relate the appearance of the fracture to the leak-rupture tendency of the component.

The first group of experiments were reported by Weed and Johnson[13]. Five 12-inch ANSI Standard B16.9 tees were tested. In all five cases the tee was subjected to a constant internal pressure, at room temperature, with water as the pressurizing medium. Tees T-4, 6, 8, and 15 were also subjected to fully reversed, out-of-plane moment loading applied to the branch pipe. Tee T-7 was loaded in-plane. Table 3 gives a more detailed account of the load values. Unfortunately, only photographs of T-4 and T-6 were available. The remaining discussion is limited to these two components.

No provision was made to maintain the internal pressure in these tests. The fact that the crack driving force was lost is confirmed by the author's remarks for tee T-4; "The internal pressure in the tee was at 1925 psig at the time of failure and a high pressure stream was expected. However, the water poured out much like water flowing from a faucet when the pressure is low."[13] Because the internal pressure was lost, the possibility of a rupture in these tests was also lost.

Although the internal pressure was lost, the general appearance of the cracked tees is interesting. All the tees failed in the region of maximum stress as determined by experimental stress analysis. In each case the cracks initiated on the outer surface and grew through-the-wall.

As noted earlier, T-4 was loaded out-of-plane with the load applied to the branch pipe. A constant internal pressure was maintained until the crack grew through-the-wall thickness. As shown in Figure 14, the crack initiated on the side of the tee and propagated well around the circumference of the tee (in the crotch region).

In the presence of the bending load this crack orientation and length might be considered critical.* It is interesting to note that

---

* The word 'critical', used in this context, implies a flaw geometry that would result in a reduction of the burst strength of the component. This is not necessarily the same as the 'critical size' discussed earlier.

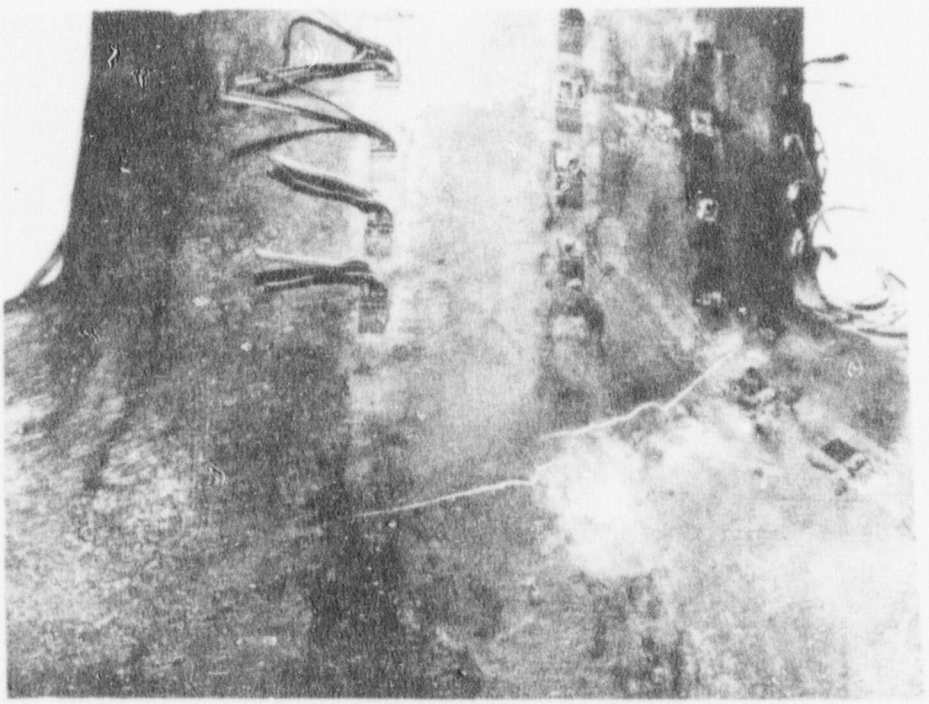

FIGURE 14. CRACK IN T-4 AFTER A LEAK FAILURE AT 2062 CYCLES[14]

examination of the interior of the tee revealed several cracks normal to the plane of the crack that caused the failure and growing outward from the inside surface. T-4 was the only specimen in this group to indicate the presence of such cracks.

Figure 15 shows the appearance of T-6 at the conclusion of the test. Although some discrepancies exist between the direction of maximum stress and the direction of crack propagation, comparison of T-4 (Figure 14) and T-6 indicates that the cracks are similar in size, location, and orientation. As for T-4, this crack orientation might be considered critical in the presence of out-of-plane bending loads.

The second group of experiments were reported by Hayes and Moore.[15] Four 24-inch ANSI Standard B16.9 tees were tested. Tees T-11, T-12, and T-13, were subjected to a cyclic internal pressure with transformer oil as the pressurizing medium. The fourth test, T-16, had a constant internal pressure (300 psig) with the cyclic stress due to fully reversed "in-plane" moment loading applied to the branch pipe. Photographs for T-11 and T-13 are the only ones included here.

Figures 16 and 17 show the appearance of the crack on the outside and inside surfaces, respectively, of T-11. The crack initiated on the inner surface in the crotch region and propagated in a direction normal to the applied hoop stress. Comparing Figures 16 and 17 shows that the crack was substantially longer on the inside surface than it appeared to be on the outer surface.

Figure 18 depicts the crack in the inside crotch region of T-13. T-12 appeared very similiar to T-11 and T-13 although T-12 is not included here.

The internal pressure was lost for these specimens once the wall was penetrated. However, the longitudinal orientation of the cracks was shown to reduce the burst strength of tee sections in the G.E. burst tests.[36] T-12 and T-13 both had cracks of this orientation and of a similiar length.

Although it is not possible to state conclusively whether the cracks were of a critical size, it is important to note that a cyclic internal pressure causes cracks that are of a critical orientation (in terms of burst test results). Further, these cracks may be substantially longer on the inner surface than they are on the outer surface.

FIGURE 15. CRACK IN T-6 AFTER A LEAK FAILURE AT 1309 CYCLES[14]

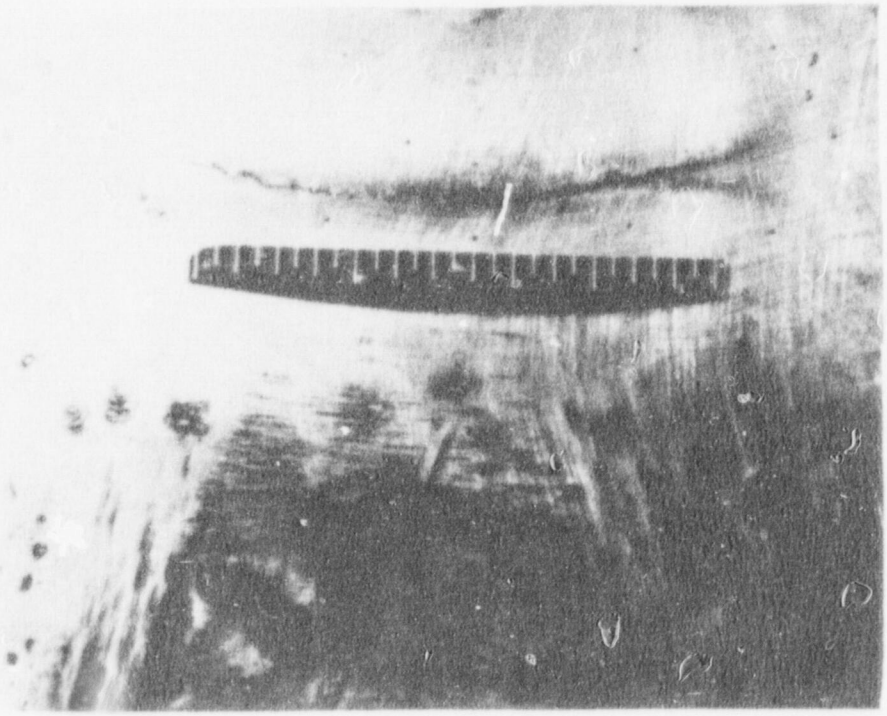

FIGURE 16. VIEW OF FATIGUE CRACK ON THE OUTSIDE SURFACE OF T-11 TEE[15]

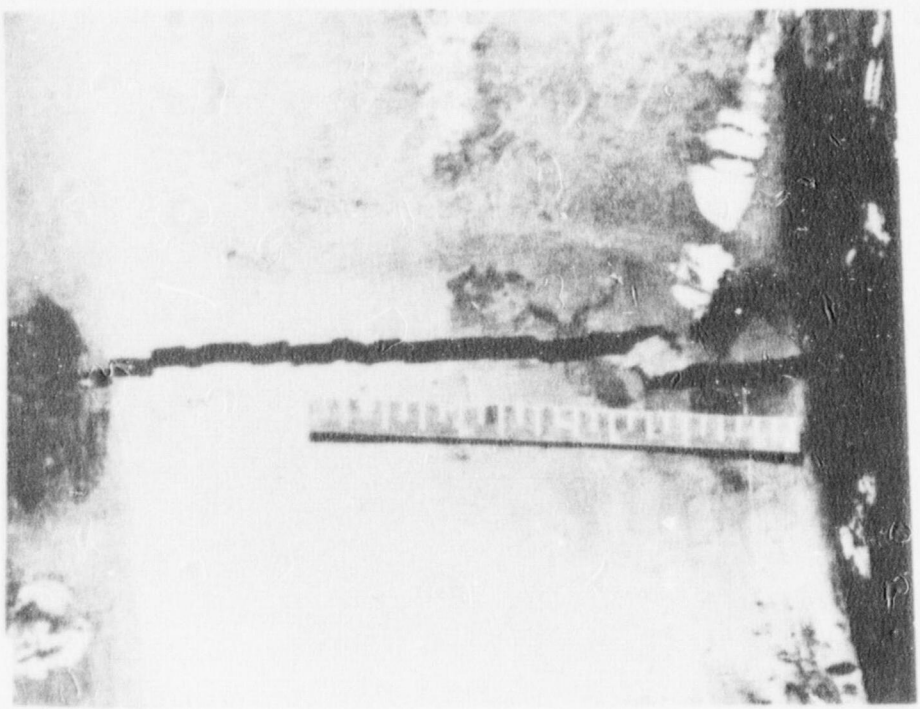

FIGURE 17. VIEW OF FATIGUE CRACK ON THE INSIDE SURFACE OF T-11 TEE[15]

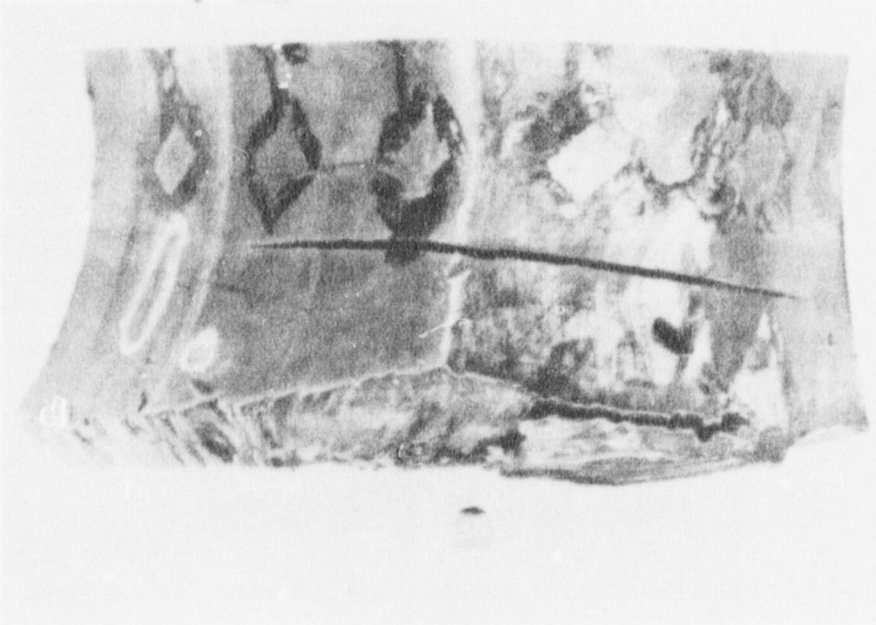

FIGURE 18. VIEW OF FATIGUE CRACK ON INSIDE SURFACE OF T-13 TEE[15]

The third group of experiments were those conducted by General Electric.[15,36,37] This group of experiments is important for two reasons. First, some of the straight pipe tests with circumferential flaws were sealed so as to maintain pressure once the wall was penetrated. Second, the moment loading was continued after the leak was observed. Because the moment loading was continued, the manner in which the flaw continues to grow may be established as well as a rough estimate of the number of cycles required to achieve substantial crack lengths. Two specific examples are used herein to illustrate the results of these tests. Three other photographs are included to illustrate the appearance of the cracks for various loading conditions.

Figure 19 shows the appearance of one circumferentially notched pipe section at the completition of the cyclic moment load test. The crack penetrated the wall at 11883 cycles. It is not clear how many cycles were applied to the specimen after the wall was penetrated. However, the authors note, "extremely large (>60 percent of the pipe circumference) circumferential cracks have been produced in the laboratory of BWR operating pressure and no sudden fracture occurred".[37] Although the PWR pressure is greater than the BWR pressure, the stress level allowed in the piping is the same for both systems. Consequently, it is not likely that a rupture would result upon wall penetration at the PWR operating conditions assuming that pressure and bending loads are the primary loadings.

Figures 20 and 21 illustrate how a crack may extend if the bending loads are not removed once the wall is penetrated. The tee section shown is CCTS-2, a 6-inch tee loaded out-of-plane with the load applied to the branch pipe.

As shown in Figure 20, the flaw that penetrated the wall had a surface length slightly greater than 1-inch. The wall of CCTS-2 was penetrated at 9367 load cycles. An additional 1082 load cycles caused the crack to extend several inches along the length of the "run" section of the tee. Figure 21 shows the appearance of CCTS-2 at the completion of testing. A total of 10449 load cycles had been imposed on the tee. Based on the results of the burst tests, a flaw in this orientation will reduce the burst strength (pressure) of a tee section. Because of the rapid rate of flaw extension once the wall has been penetrated, it is not possible to state conclusively that a

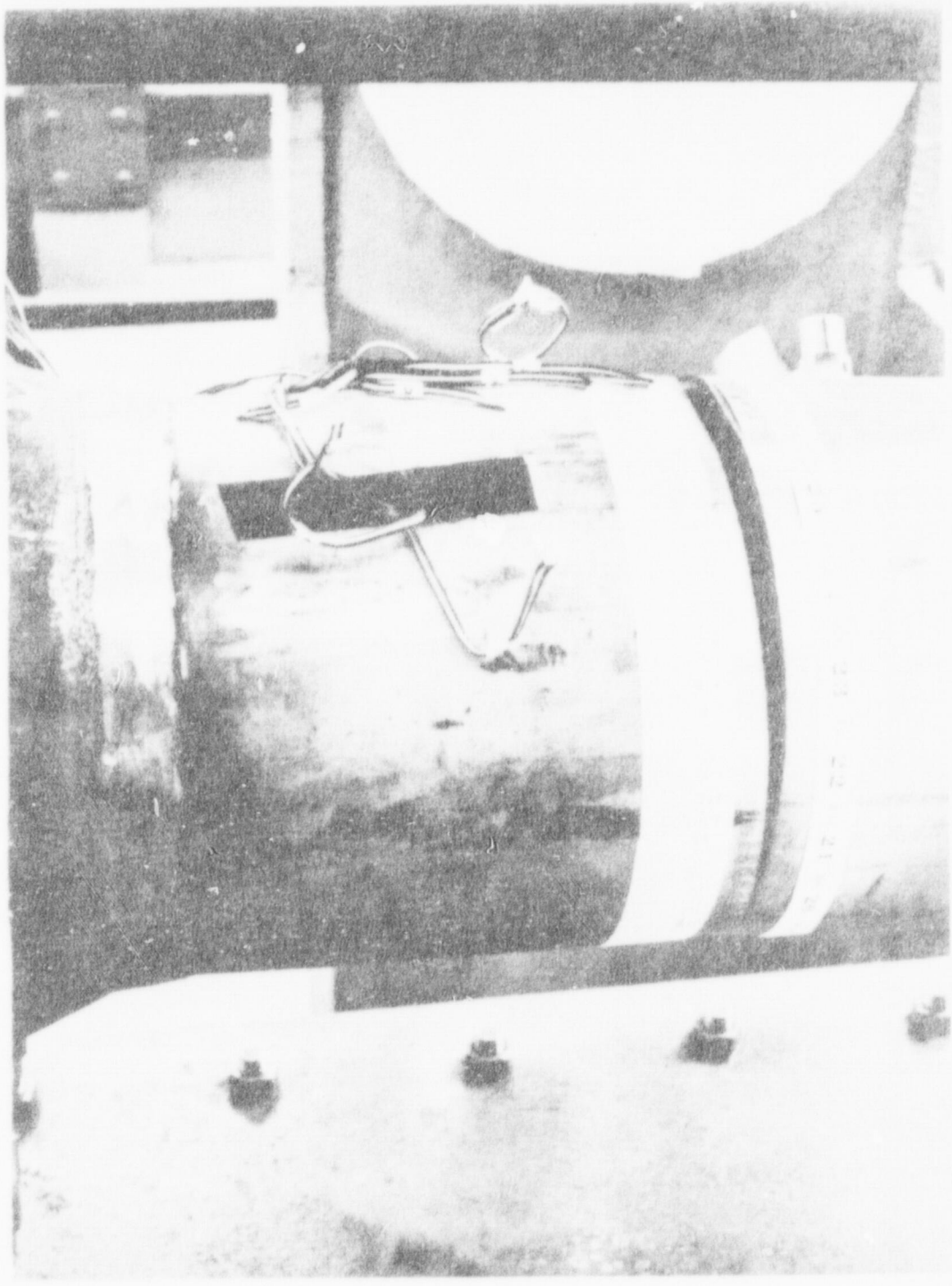

FIGURE 19. FINAL FRACTURE, STAINLESS STEEL, ROOM TEMPERATURE (CSS-25)[36]

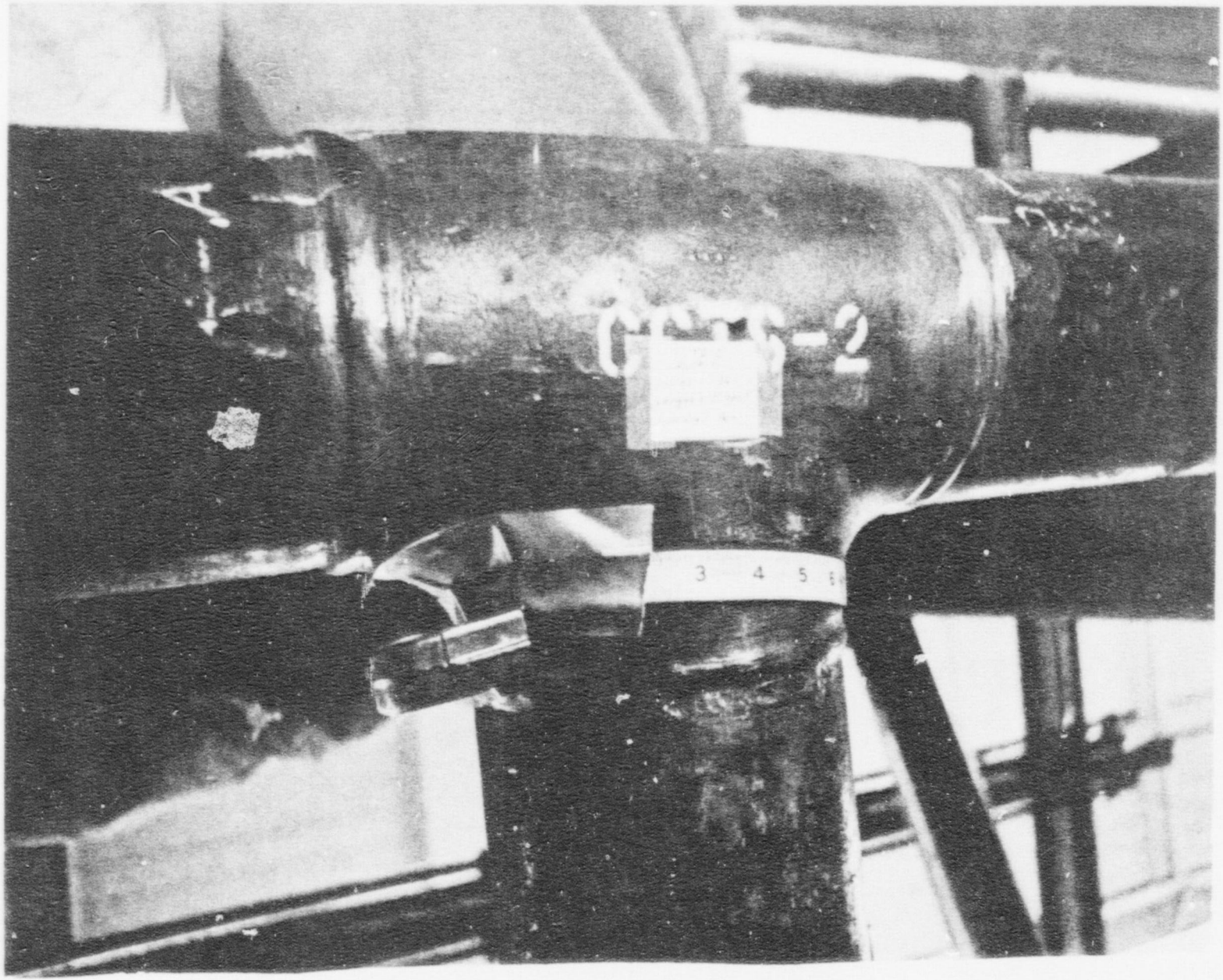

FIGURE 20. THROUGH WALL PENETRATION, SPECIMEN NO. CCTS-2. VIEW SHOWS BOTTOM SIDE OF SPECIMEN[37]

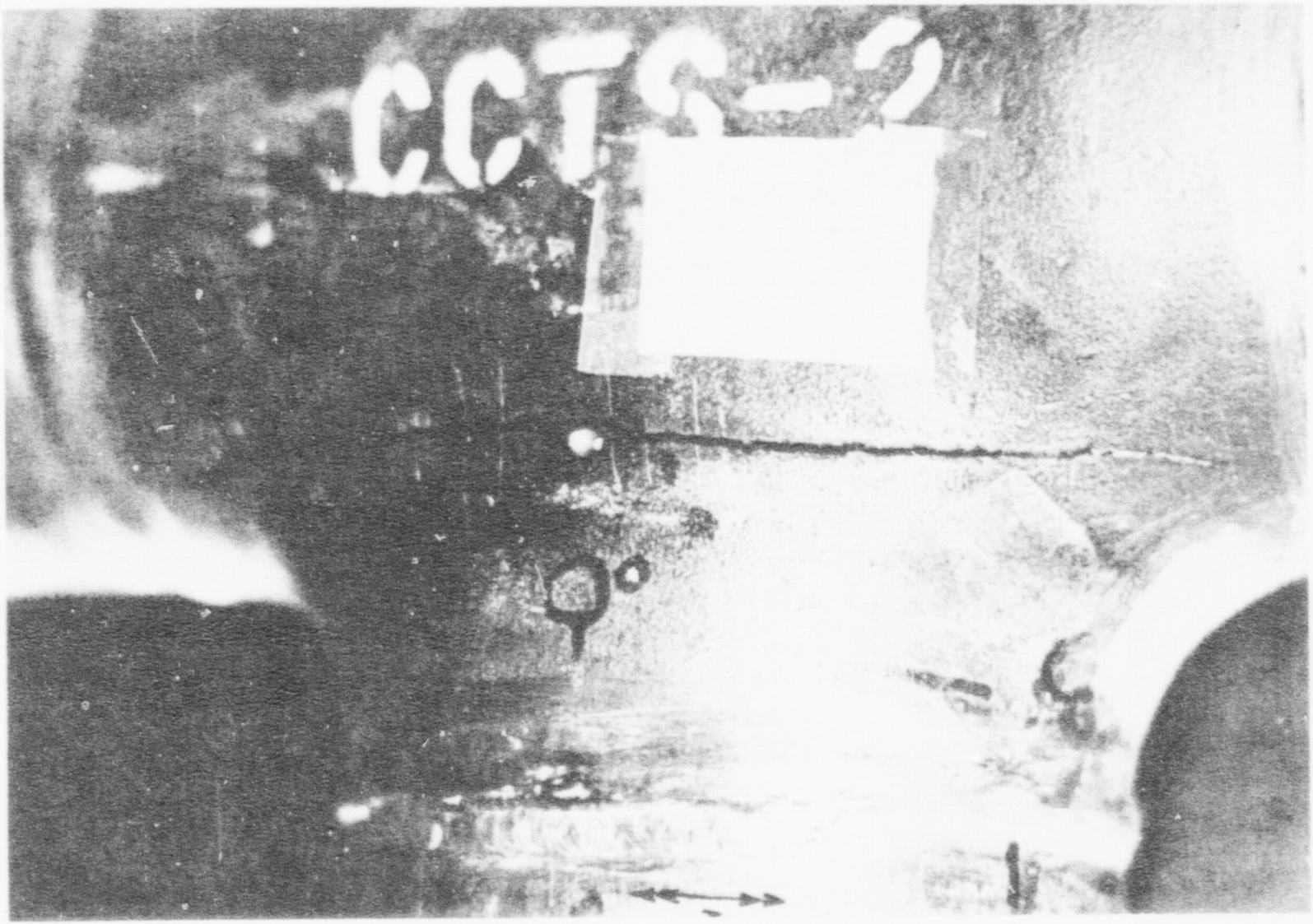

FIGURE 21. FINAL FRACTURE GEOMETRY, SPECIMEN NO. CCTS-2. VIEW SHOWS BOTTOM SIDE OF TEE[37]

leak could be detected and the reactor shut-down before such a flaw grew to a size that would result in a rupture.*

From an operational viewpoint, it is important to note that moment loadings are not necessarily lost once a leak has been detected in a nuclear piping system. Even if a flaw is not large enough to present a threat of rupture once it grows through-the-wall, continued moment loading may well extend the flaw length to the point where rupture is a very real possibility.

Figures 22, 23, and 24 illustrate how flaws may continue to grow for a variety of component geometries and load types.

Figure 22 shows a 6-inch elbow that was loaded in-plane. The flaw extends the full length of the side of the elbow, through the weld line on each end, and into the pipe sections attached to the elbow. As was noted in Section 3.1.2, a flaw in this orientation behaves something like an axial flaw in straight pipe. The flaw depicted in Figure 22 lies essentially perpendicular to the direction of the principal stress for a pressure loading and thus may substantially reduce the pressure carrying capacity of the elbow.

Figure 23 shows a 6-inch tee that was loaded in-plane with the load applied to the run pipe. The flaw extends along the axis of the branch pipe well into the body of the tee. As may be noted in Figure 23, the flaw has extended past the weld line for the branch connection and into the branch pipe. Even if this flaw geometry did not reduce the pressure carrying capacity of the tee, the extension of the flaw into the branch pipe in an axial orientation may result in a rupture of the pipe before the tee. This possibility depends on the factors discussed in Section 3.1.

Figure 24 shows a 6-inch tee that was loaded in-plane with the load applied to the branch pipe. The tee was cracked well around the circumference in the crotch region. Additional cracks may be observed in the 'run' section of the tee. These cracks are essentially at 45 degrees to the run pipe axis. One of these flaws joins the circumferential flaw on the crotch region and extends into the run pipe weld line.

---

* This discussion assumes that operating pressure is somehow maintained in the operating reactor even after the wall has been penetrated.

FIGURE 22. ELBOW IN-PLANE COMPLETION OF TEST(37)

FIGURE 23. TEE, LOADED IN-PLANE (RUN), AT COMPLETION OF TEST[37]

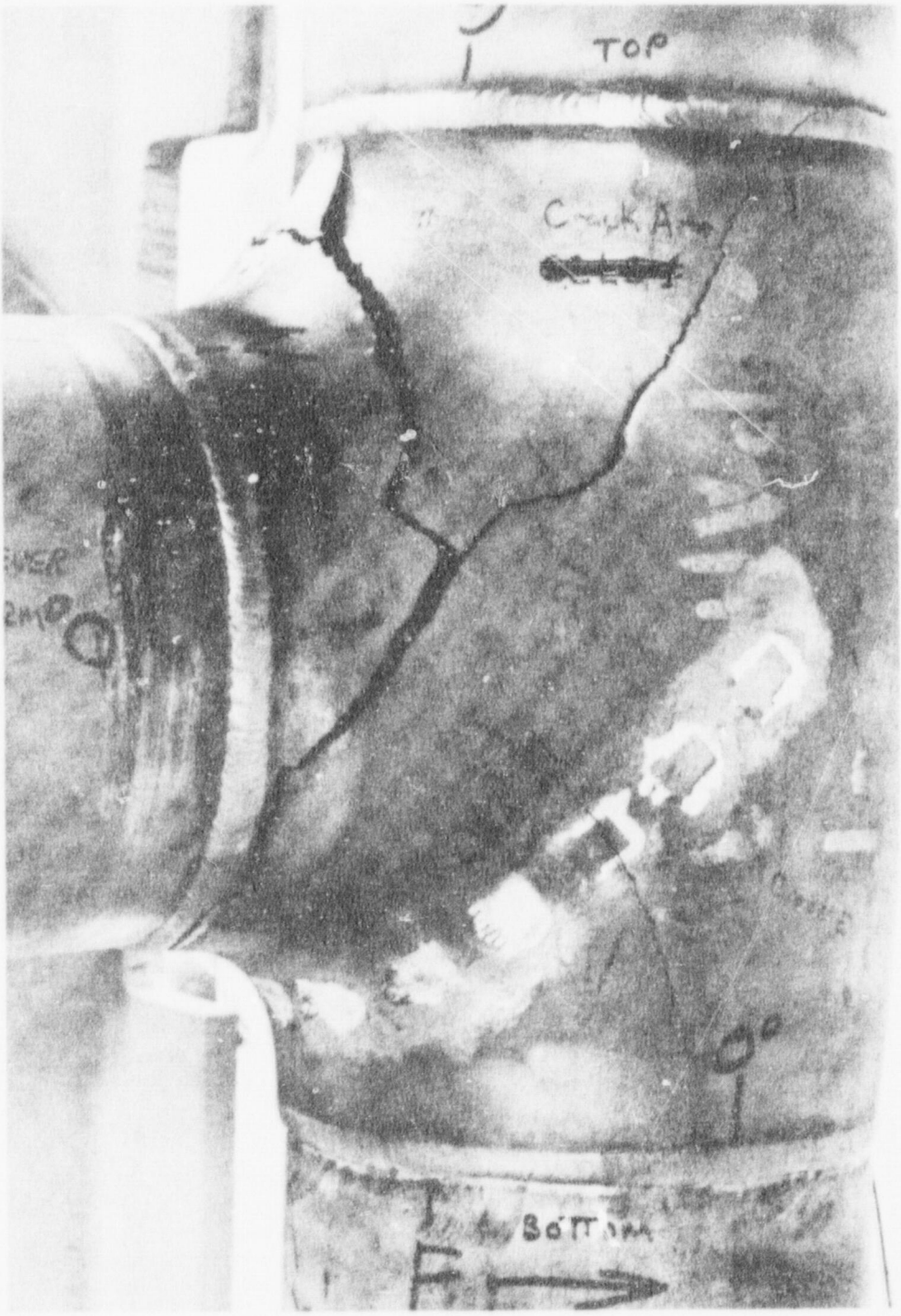

FIGURE 24. TEE, LOADED IN-PLANE (BRANCH), AT COMPLETION OF TEST[37]

3.4 Summary

Although it is impossible to make definitive statements regarding the leak rupture evaluation for most of the tests noted in Section 2 of this report, some important points have been noted.

(1) Circumferential flaws in straight pipe attain a substantial length (>60 percent of the circumference) without rupturing at BWR conditions. From this it may be inferred that a leak could be detected and a safe shut down performed at PWR pressures.

(2) Cyclic pressure loading on tees produces cracks that are of a critical orientation (in terms of the burst test results) and that are quite long on the inner surface before they penetrate the full wall thickness.

(3) Out-of-plane moment loading on tees produces cracks that are of a critical orientation and that might grow to a critical size in a few loading cycles once the wall has been penetrated.

(4) In-plane moment loading on tees produces cracks that are not of a particularly critical orientation (in terms of burst test results). However, these cracks may extend well around the circumference of the crotch region before they penetrate the full wall thickness.

(5) In-plane moment loading on elbow sections produces cracks that lie essentially perpendicular to the direction of the principal stress for a pressure loading and may reduce the pressure carrying capacity of the elbow. The cracks generated by such loadings tend to propagate across the weld line and into the attached straight pipe sections thereby raising the possibility of a longitudinal rupture in the straight pipe section (see Figure 22).

(6) Other component types have not been considered in this analysis simply due to a lack of photographs of such test components.

A better assessment of the leak rupture tendencies of piping and piping components could be made if experiments were conducted in which the pressure was maintained and the test temperature was above room temperature, i.e., 550 F.

4.0 IMPLICATIONS ON COLD LEG PIPING

The tests discussed in Sections 2 and 3 of this report all dealt with pipe sections that were substantially smaller in size than typical sections of the cold leg piping system. The largest tees examined were the 24-inch-diameter tees examined by Hayes and Moore[15]. The other sizes ranged between 4- and 12-inch-diameter.

The Code procedures for analyzing fatigue life should provide nominal stress values that are insensitive to size variations. However, the differences between small components (4-inch) and the full-scale structure, in terms of geometric similarities, relative sizes, and environmental considerations, gives rise to the issue of similitude, i.e., are the results for small-scale tests truly comparable to full-scale behavior.

The remainder of this section considers to what extent the results of these small-scale tests may be applied to the cold leg piping system.

4.1 Description of the Cold Leg Piping System

The cold leg piping system may be defined as the group of piping components installed between the outlet nozzel of the main coolant pump and the inlet nozzel of the reactor vessel. Typically, the cold leg consists of a length of 30-inch-diameter pipe (2.5-inch nominal wall thickness) with one or more branch connections along the length of the pipe. Elbow sections are utilized as necessary to complete the system.

The piping system may be made from 'clad' piping (ferritic steel pipe with stainless steel cladding) or in some cases the piping is all stainless steel.

The cold leg is exposed to a water environment with a nominal temperature of 550 F. The nominal internal pressure is 2,500 psig. The stress level will vary depending on the power level fluctuations the plant experiences.

Cumulative fatigue damage is evaluated using a linear damage concept. Although this technique is not as sophisticated as some of the recently developed techniques for evaluating fatigue crack growth rates when a load

spectrum is imposed, the linear damage concept should provide conservative results for the fatigue life evaluation of piping components.

4.2 The Question of Similitude

The concept of using 'small-scale' tests in the evaluation of large systems is a standard practice employed in virtually all sciences. The benefits of such tests are directly related to how well the test simulates full-scale behavior. If similitude does not exist between the test structure and the full-scale structure then the value of the test results will be questionable.

Several questions arise in trying to establish whether or not similitude exists for the piping component fatigue tests considered herein and the cold leg piping. Several areas of concern are listed below;

(1) Geometric similitude

(2) 'Size' effect

(3) Test environment versus operating environment

(4) Effect of accelerated testing.

Each of these items will be discussed in the following subsections.

4.2.1 Geometric Similitude. There are essentially three types of components to be considered as important to the cold leg; (1) girth butt welds, (2) elbows, and (3) branch connections. The girth butt welds in the test components were 'field welds', i.e., welds made by hand employing a series of weld 'passes' that serve to bond the two components together. However, most of the welds in the cold leg are of the double submerged arc-weld type made in a much more controlled fashion and should represent a superior quality band. Even the field welds that are necessary to complete the cold leg should represent a band of at least similar quality to those in the test specimens. Thus, it is a safe assumption that geometric similitude exists for girth butt welds.

The elbow sections used in the cold leg piping are manufactured by a process that is very similiar to the one used to manufacture small-scale components. The ratios of diameter to thickness and bend radius to cross-

sectional radius are quite similar for the small- and large-scale components. Thus, to assume that geometric similitude exists for the elbow sections is not unrealistic.

The branch connections tested may not be exactly similar to those in the cold leg. However, the additional reinforcement required for branch connections in the cold leg should make the cold leg behavior conservative with respect to the fatigue test results.

4.2.2 'Size' Effect. It may be postulated that a large component will have a longer fatigue life than a small component when both are subjected to the same stress level, all other factors being equal. This effect is due to the fact that a similar number of cycles would be required to initiate a crack in both components but that a greater number of cycles would be required to propagate the crack to failure for the large component than for the small one, i.e., the crack must extend further by virtue of the increased wall thickness. Although this argument is reasonable, comparisons of the tests reviewed in Section 2 of this report do not indicate that such an effect is a reality. If such an effect is not observed when comparing 4-inch components to 24-inch components, there is no reason to expect any appreciable effect in the 30-inch components.

4.2.3 Test Environment Versus Operating Environment. As noted in Section 4.1, the cold leg piping is exposed to a water environment, a nominal temperature of 550 F and a nominal pressure of 2500 psig. The test specimens were subjected to a variety of environments although none of them were as severe as the PWR environment.

Based on the comparisons of test environments to the actual PWR environment, the test results may be nonconservative with respect to the cold leg piping.

4.2.4 Effect of Accelerated Testing. The effect of accelerated testing is most noticeable when considering the time-dependent factors that may alter the fatigue life of a component. Perhaps the most obvious of such factors is corrosion. Both corrosion assisted fatigue and stress-corrosion cracking are time-dependent. For corrosion assisted fatigue crack growth, the

lower the cyclic frequency the more noticeable the effect of the environment. Stress-corrosion cracking is also a time-dependent process. It is highly unlikely that a stress-corrosion crack could be a factor in the fatigue test results due to the short duration of the tests. However, in the projected 40 year life of a PWR power plant, stress-corrosion cracking could become a significant factor.

Because of the time-dependent factors involved, such as corrosion-stress interactions, the accelerated fatigue test results may be nonconservative with respect to the cold leg piping.

4.3 Additional Considerations and Results

One point that was not discussed in the previous section is the influence of the stainless steel cladding on ferritic steel pipe. It is the contention of this report that the cladding

(1) Does not affect the geometric similarities discussed,

(2) Has no bearing on any size effects, and

(3) Will be more resistant to the environmental attack than the base metal (ferritic steel).

In general, the cladding should have no detrimental effects on the behavior of the piping and may retard environmental attack.

Another point not to be overlooked is that the fatigue tests evaluated in Section 2 of this report generally involved tests where $S_n/3S_m > 1$. As noted previously, as this ratio increases the K_e factor tends to over compensate resulting in very high N_t/N_c ratios, i.e., the Code conservatism increases. However, cold leg piping stress levels will generally be below 3 S_m. This implies that the factor of safety for 'normal' cycles will not be overly conservative and that the postulated large amplitude cycles will not be as damaging as predicted.

Loading type is another point. The pressure cycle test on the forged welding tee, T-11 (Table 5), indicate that the results for cyclic pressure loadings may not be conservative. Specifically, the N_t/N_c ratio for this test was 5.2, well less than the value of 20 established as the minimum conservative value. Although forged welding tees are not employed in the cold

leg piping system, this test illustrates a potential problem in the Code analysis for cyclic pressure loadings. It appears that the Code analysis is at least conservative for other load types. In fact, the analysis may be overly conservative in some instances.

Some general conclusions may be reached after considering the above discussion and the results of the fatigue tests.

(1) The Code analysis is very conservative for stress intensities exceeding 3 S_m. This will be true regardless of the other factors involved, implying that the postulated large amplitude events will not be as damaging as the analysis predicts.

(2) The Code analysis for pressure loadings should be reviewed.

(3) Straight piping sections can tolerate long circumferential cracks so long as pressure is the only loading. This characteristic should be true regardless of the pipe size.

(4) Environmental factors are not considered in the Code analysis. This point is perceived as a short coming of the Code approach and may well result in unacceptable behavior of the cold leg piping system. This behavior might be in the form of premature crack initiation (due to stress-corrosion cracking or simply general corrosion) and accelerated rates of crack growth.

(5) The results of the fatigue tests on piping components indicate that the fatigue analysis of the cold leg piping system should be conservative. However, this result could be changed due to environmental factors. The impact of such factors on the Code analysis cannot be assessed at the present time.

Clearly, the analysis of the fatigue life of the cold leg piping system is a complex problem. The complete solution of this problem may well require more than a simplified analysis technique.

5.0 SUMMARY AND CONCLUSIONS

This report sought to evaluate the results of fatigue tests on piping components in an effort to;

(1) Determine the margin of safety of the present ASME code method of evaluation.

(2) Determine the leak-rupture trends of components tested with significant internal pressures.

(3) Determine the implications of the tests with respect to the cold leg piping systems in PWR's.

Section 2 of this report dealt with the evaluation of the margin of safety (N_t/N_c) for the fatigue tests. The majority of these tests were conducted with $S_n > 3S_m$. This section of the report is basically an extension of Phase Report 115-10[10], and as such includes some sections of that report essentially unchanged.

The four main conclusions of Section 2 are:

(1) In general, the conservatism of the ASME code evaluation procedure is acceptable with $S_n > 3S_m$.

(2) The Code evaluation procedures for cyclic pressure loadings should be reviewed. This conclusion is based on the results of the cyclic pressure test of T-11 (Table 5).

(3) The K_e factor tends to overcompensate as S_n goes well above $3S_m$ resulting in margins of safety two orders of magnitude greater than the assumed value of 20 in some cases.

(4) The Code analysis is generally more conservative for ferritic steel than for stainless steel.

Section 3 of this report sought to evaluate the leak-rupture trends of the various components tested in terms of the appearance of the fractures. The appearance of components fracture in burst tests were reviewed. Then, the appearances of the fractured fatigue test components were compared to the burst test components. Although no definitive assessment of the leak-rupture trends was possible, several conclusions were made. These are:

(1) Circumferential flaws in straight pipe attain a substantial length (> 60 percent of the circumference) without rupturing at BWR conditions. From this it may be inferred that a leak could be detected and a safe shut down performed at PWR pressures.

(2) Cyclic pressure loading on tees produces cracks that are of a critical orientation (in terms of the burst test results) and that are quite long on the inner surface before they penetrate the full wall thickness.

(3) Out-of-plane moment loading of tees produces cracks that are of a critical orientation and that might grow to a critical size in a few loading cycles once the wall has been penetrated.

(4) In-plane moment loading on tees produces cracks that are not of a particularly critical orientation (in terms of burst test results). However, these cracks may extend well around the circumference of the crotch region before they penetrate the full wall thickness.

(5) In-plane moment loading on elbow sections produces cracks that lie essentially perpendicular to the direction of the principal stress for a pressure loading and may reduce the pressure carrying capacity of the elbow. The cracks generated by such loadings tend to propagate across the weld line and into the attached straight pipe sections thereby raising the possibility of a longitudinal rupture in the straight pipe section. (See Figure 22).

(6) Other component types have not been considered in this analysis simply due to a lack of photographs of such test components.

Section 4 of this report attempted to evaluate the implications of the fatigue test results on the cold leg piping system. A key point in that section involved the similitude between the small-scale fatigue tests and the full-scale cold leg piping. Geometric similitude, size effect, test environment, and effect of accelerated testing were examined in detail.

The general conclusions were that the behavior of the cold leg piping would be conservative with respect tc the fatigue test results. The most important discrepancy exists in assessing the effect of the environment over the 40 years of PWR plant life. If the environmental attack is significant, the cold leg behavior may not be conservative with respect to the fatigue test results. To accurately evaluate the margin of safety inherent in the cold leg piping, an analysis technique that accounts for the environmental factors must be employed.

6.0 REFERENCES

(1) ASME Boiler and Pressure Vessel Code, Section III, Division 1, "Nuclear Power Plant Components", Subsection NB, 1977.

(2) "Criteria of the ASME Boiler and Pressure Vessel Code for Design by Analysis in Sections III and VIII, Division 2", ASME, New York.

(3) Appendix 1, ASME Boiler and Pressure Vessel Code, Section III, Division 1, "Nuclear Power Plant Components", Subsection NB, 1977.

(4) Moore, S. E., Bryson, J. W., "Design Criteria for Piping and Nozzles Program Quarterly Progress REport for April-June, 1976, ORNL/NUREG/TM-91, Oak Ridge National Laboratory, February, 1977.

(5) ASME Boiler and Pressure Vessel Code, Section III, Division 1, "Nuclear Power Plant Components", Subsection NB, Table NB-3682.2-1, 1977.

(6) Markl, A.R.C., "Fatigue Tests of Piping Components", Trans. ASME, Volume, 74, pp 287-303 (1952).

(7) Heald, J. D., and Kiss, E., "Low Cycle Fatigue of Prototype Pipe Components", General Electric (San Jose) Report 10763, January, 1973.

(8) Kiss, E., Heald, J. D., and Hale, D. A., "Low-Cycle Fatigue of Prototype Piping", General Electric (San Jose) Report GEAP-10135, January, 1970.

(9) Heald, J. D., Kiss, E., "Low Cycle Fatigue of Nuclear Pipe Components", Journal of Pressure Vessel Technology, August, 1974.

(10) Rodabaugh, E. C., and Moore, S. E., "Phase Report No. 115-10 on Comparisons of Test Data with Code Methods for Fatigue Evaluation", ORNL-TM-3520, Oak Ridge National Laboratory, November, 1971.

(11) Markl, A.R.C., "Fatigue Tests of Welding Elbows and Comparable Double-Mitre Bends", Trans. ASME, Vol. 69, pp 869-879 (1947).

(12) Udoguchi, T., Asada, Y., "Investigation of Low Cycle Fatigue Strength of Piping Components", 2nd International Conference on Pressure Vessel Technology, Proceedings and Papers, San Antonio, Texas, October, 1973.

(13) Greenstreet, W. L., Moore, S. E., and Callahan, J. P., "1970 Annual Progress Report on Studies in Applied Solid Mechanics (Nozzles and Piping Components)", Oak Ridge National Laboratory, to be published.

(14) Weed, R., Johnson, N., "Experimental Stress Analysis and Fatigue Test of ANSI Standard B16.9 Tees", Volume 1, ORNL Sub-4356, Report No. 1, Volumbue 1, Oak Ridge National Laboratory.

(15) Hayes, J. K., Moore, S. E., "Experimental Stress Analysis of Four 24-inch ANSI Standard B16.9 Tees", Journal of Pressure Vessel Technology, November, 1973.

(16) Grigory, S. C., "Studies of the Fatigue Strength of Pressure Vessels, Fatigue Tests of One-Half Scale Model Pressure Vessels", April 29, 1968, Southwest Research Institute, San Antonio, Texas, to USAEC.

(17) Cook, T. R., "Studies on the Fatigue of Branched Connections Related to the Shakedown Pressure", 3rd International Conference on Pressure Vessel Technology, Tokyo, Japan, 1977.

(18) Markl, A.R.C., and George, H. H., "Fatigue Tests on Flanged Assemblies", Trans. ASME, Vol. 72, pp 77-87 (1950).

(19) Pickett, A. G., and Grigory, S. C., "Studies of the Fatigue Strength of Pressure Vessels, Part 1. Cyclic Pressure Tests of Full-Size Pressure Vessels", September, 1966, Southwest Research Institute, San Antonio, Texas, to USAEC.

(20) Kameoka, T., Sato, E., An, B., and Sato, Y., "Low-Cycle Fatigue of Pressure Vessels with Butt-Welded Nozzles", Proceedings of First International Conference on Pressure Vessel Technology, Delft, 1969, Available from ASME, 345 E. 47th Street, New York, N.Y.

(21) Rodabaugh, E. C., "Stresses in Out-of-Round Pipe Due to Internal Pressure, ORNL-TM-3244, January, 1971.

(22) Stewart, W. C., and Schreitz, W. G., "Thermal Shock and Other Comparison Tests of Austenitic and Ferritic Steels for Main Steam Piping", Trans. ASME, Vol. 72, pp 1051-1072 (1950).

(23) Weisberg, H., and Soldan, H. M., "Cyclic Heating Test of Main Steam Piping Materials and Welds at the Sewarin Generating Station", Trans. ASME, Volume 76, pp 1085-1091 (1954).

(24) Tidball, R. A., and Shrut, M. M., "Thermal-Shocking Austenitic Stainless Steels with Molten Metals", Trans. ASME, Volume 76, pp 639-643 (1954).

(25) Gysel, W., Werner, A., and Gut, K., "Thermal Shock Behavior of Various Grades of Cast Steel", Proceedings of Joint International Conference on Creep, Institute of Mechanical Engineers, London, pp 3-33 to 3-41 (1963).

(26) Schneider, P. J., "Temperature Response Charts", John Wiley & Sons, 1963.

(27) Miyazono, S., Ueda, S., Kodaira, T., Shibata, K., Isozaki, T., and Nakajima, N., "Fatigue Behavior of Nozzles of Light Water Reactor Pressure Vessel Model", 3rd International Conference on Pressure Vessel Technology, Tokyo, Japan, 1977.

(28) Fujimura, T., Miyazono, S., Kodaira, T., and Shibata, K., "Integrity Assessment of Structural Models of a Reactor Vessel with Notched Nozzles Under Cyclic Pressure Loading", 2nd International Conference on Pressure Vessel Technology, Proceedings and Papers, San Antonio, Texas, October 1973.

(29) Rodabaugh, E. C., Maxey, W. A., and Eiber, R. J., "Review and Assessment of Research Relevant to Design Aspects of Nuclear Power Plant Piping Systems", NUREG-0307, U.S. Nuclear Regulatory Commission, July 1977.

(30) Eiber, R. J., Maxey, W. A., Duffy, A. R., and Atterbury, T. J., "Investigation of the Initiation and Extent of Ductile Pipe Rupture", BMI-1866, July, 1969.

(31) "Reactor Primary Coolant System Rupture Study Quarterly Progress Report No. 16", GEAP-10024, AEC Research and Development Report, April, 1969.

(32) Maxey, W. A., Kiefner, J. F., Eiber, R. J., and Duffy, A. R., "Ductile Fracture Initiation, Propagation, and Arrest in Cylindrical Vessels", Fracture Toughness, Proceedings of the 1971 National Symposium on Fracture Mechanics, Part II, ASTM STP 514, American Society for Testing and Materials.

(33) Kiefner, J. F., Maxey, W. A., Eiber, R. J., and Duffy, A. R., "Failure Stress Levels of Flaws in Pressurized Cylinders", Progress in Flaw Growth and Fracture Toughness Testing, ASTM STP 536 American Society for Testing and Materials.

(34) Fourth Symposium on Line Pipe Research, presented by the Pipeline Research Committee of the American Gas Association, Dallas, Texas, November 18-19, 1969.

(35) Eiber, R. J., Maxey, W. A., and Duffy, A. R., and Atterbury, T. J., "Investigation of the Initiation and Extent of Ductile Pipe Rupture", Final Report, Task 17, June, 1971.

(36) "Reactor Primary Coolant System Rupture Study Quarterly Report No. 20, January-March, 1970", GEAP-11069, AEC Research and Development Report, April 1970.

(37) Kiss, E., Heald, J. D., and Hale, D. A., "Low Cycle Fatigue of Prototype Piping", GEAP-10135, AEC Research and Development Report, January, 1970.

(38) Wilkowski, G. M., and Eiber, R. J., "Review of Fracture Mechanics Approaches to Defining Critical Size Girth Weld Discontinuities", Welding Research Council Bulletin No. 239, July 1978.

NRC FORM 335 (7-77)

U.S. NUCLEAR REGULATORY COMMISSION

BIBLIOGRAPHIC DATA SHEET

1. REPORT NUMBER (Assigned by DDC)
NUREG/CR-0325

4. TITLE AND SUBTITLE (Add Volume No., if appropriate)
Relevance of Fatigue Tests to Cold Leg Piping

2. (Leave blank)

3. RECIPIENT'S ACCESSION NO.

7. AUTHOR(S)
M. E. Mayfield, E. C. Rodabaugh and R. J. Eiber

5. DATE REPORT COMPLETED
MONTH: July YEAR: 1978

9. PERFORMING ORGANIZATION NAME AND MAILING ADDRESS (Include Zip Code)
Battelle Columbus Laboratories
505 King Avenue
Columbus, OH 43201

DATE REPORT ISSUED
MONTH: August YEAR: 1978

6. (Leave blank)

8. (Leave blank)

12. SPONSORING ORGANIZATION NAME AND MAILING ADDRESS (Include Zip Code)
Metallurgy & Materials Research Branch
Division of Reactor Safety Research
USNRC
Washington, D. C. 20555

10. PROJECT/TASK/WORK UNIT NO.

11. CONTRACT NO.
NRC-04-76-293-03

13. TYPE OF REPORT
Final Report

PERIOD COVERED (Inclusive dates)

15. SUPPLEMENTARY NOTES

14. (Leave blank)

16. ABSTRACT (200 words or less)

The "cold leg" in a PWR, for the purpose of this report, is defined as that portion of the primary coolant loop that lays between the coolant pump and the reactor vessel. One of the conditions which may lead to failure in a cold leg consists of repeated cycles of stress. These repeated stress cycles may cause the growth of any small defect in the weld or base material and, if the stress cycles are high enough and frequent enough, the defect may grow until it penetrates the wall, resulting in a leak, or under some postulated conditions, a large break might occur. The objective of this report is to present an evaluation of available fatigue test data on piping products to: Determine the margin of safety of the present ASME code method of evaluation, Determine the leak-rupture trends of components tested with significant internal pressures, Determine the implications of the tests with respect to the cold leg piping systems in PWR's.

17. KEY WORDS AND DOCUMENT ANALYSIS

17a. DESCRIPTORS

17b. IDENTIFIERS/OPEN-ENDED TERMS

18. AVAILABILITY STATEMENT
Unlimited

19. SECURITY CLASS (This report)
Unclassified

21. NO. OF PAGES

20. SECURITY CLASS (This page)
Unclassified

22. PRICE
$

UNITED STATES
NUCLEAR REGULATORY COMMISSION
WASHINGTON, D. C. 20555

OFFICIAL BUSINESS
PENALTY FOR PRIVATE USE, $300

POSTAGE AND FEES PAID
U.S. NUCLEAR REGULATORY
COMMISSION

U.S. MAIL

120555011232 1 RSAN
US NRC
ADM DIST SERV BRANCH - SHELF
016 DC 20555
WASHINGTON